PERGAMON

Journal of Structural Geology 24 (2002) 609–635

JOURNAL OF STRUCTURAL GEOLOGY

www.elsevier.com/locate/jstrugeo

Syn-tectonic sedimentation associated with three-dimensional fault-bend fold structures: a numerical approach

Asdrúbal Bernal, Stuart Hardy*

Basin and Stratigraphic Studies Group, Department of Earth Sciences, University of Manchester, Manchester M13 9PL, UK

Received 31 July 2000; revised 26 January 2001; accepted 11 April 2001

Abstract

Syn-tectonic sediments (growth strata) in compressional structures are three-dimensional (3D) features whose geometry reflects both the style of deformation and the distribution of accommodation space in the system. Previously, numerical modelling of growth strata in compressional settings has generally been done in two-dimensions in the plane of the transport direction. In contrast, in this paper we examine growth strata associated with a 3D fault-bend fold that exhibits variations in slip along-strike. A forward numerical modelling approach is used to investigate the 3D geometry of syn-tectonic sediments under a variety of conditions.

We consider a fault-bend fold in which slip decreases linearly from the centre of the structure to zero displacement at the edges in a direction perpendicular to transport. We make use of kink-band kinematics to describe the growth of the structure. Two specific models are presented, which consider both (1) background (regional) sedimentation and (2) local erosion, transport and sedimentation. The first model approximates structures developed in submarine environments where structural growth may lead to the development of a bathymetric high. The model shows considerable lateral changes in the geometries of growth strata along the structure, with unconformities being limited to regions of high displacement, and with growth triangles being variably developed, but in some circumstances difficult to recognise. The subaerial model approximates structures developed in settings where sediments simply aggrade to the local base level. In this model, unconformities are much more prominent as growth sedimentation is often limited to regions of lower displacement.

The results presented here emphasise the utility of using 3D information on stratigraphic architectures to decipher the growth style and deformational history of natural structures. In particular, we show that cross-sections oblique to the transport direction may contain complex and highly variable pre- and syn-tectonic geometries that reflect both kink-band migration and limb rotation. The use of oblique two-dimensional (2D) information to interpret 3D structures could produce misinterpretations if the complexities of stratigraphic configurations in three-dimensions are not taken into account.

Keywords: Syn-tectonic sedimentation; Three-dimensional fault-bend fold structures; Growth strata

1. Introduction

The analysis of syn-tectonic sediments (growth strata) has recently developed into an important area of research in integrated structural geology and stratigraphy (e.g. Suppe et al., 1991; Poblet and Hardy, 1995). This arises because syn-tectonic sediments have the potential to record the interplay between structural and stratigraphic processes in a range of geological settings (e.g. Suppe et al., 1991; Gawthorpe et al., 1997). Geometries of growth strata clearly reflect the distribution of accommodation space, primarily as a result of tectonic uplift and local/regional base level change, the style of deformation, and various sedimentological processes (e.g. erosion, transport and deposition). This paper addresses the growth of compressional fault-bend folds in three dimensions and illustrates some possible geometries of growth strata associated with such structures.

Analysis of syn-tectonic sedimentation in contractional settings by numerical modelling, seismic and outcrop studies has been done at both basin (e.g. Flemings and Jordan, 1990; Chalaron et al., 1996; Garcia-Castellano et al., 1997) and map scale (e.g. Zoetemeijer et al., 1992, 1993; Poblet and Hardy, 1995). Most of these studies have been done in two dimensions, even though most authors agree that a three-dimensional (3D) analysis is critical in understanding natural structures (e.g. Wilkerson et al., 1991). The challenge is to use stratigraphic architectures preserved around ancient structures to better understand their evolution through space and time. However, nature rarely provides ideally-oriented (2D) dip and strike sections, thus, it is crucial to understand and properly interpret the geometric expression of growth strata in oblique sections. Information from outcrop studies in three dimensions also is

* Corresponding author.
E-mail address: shardy@fs1.ge.man.ac.uk (S. Hardy).

0191-8141/02/$ - see front matter
PII: S0191-8141(01)00112-2

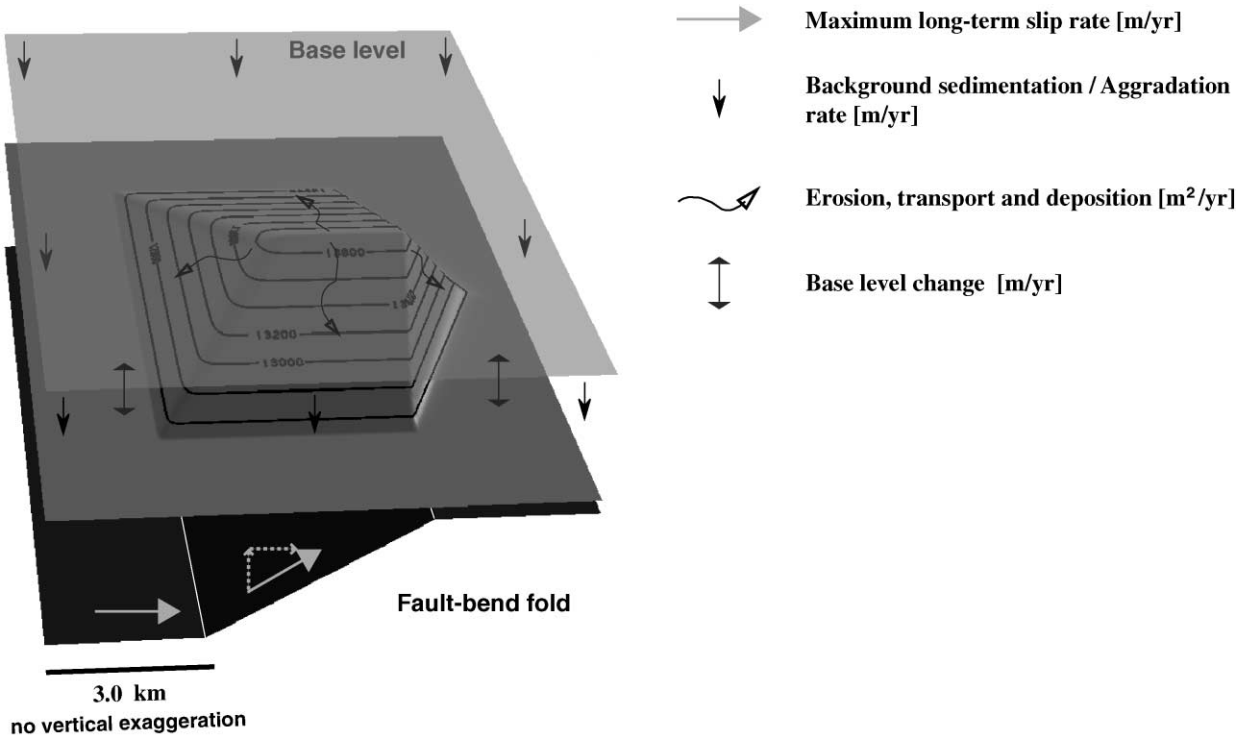

Fig. 1. Sedimentary and structural parameters defined in the numerical modelling approach. Three key processes are considered: (1) tectonic deformation (fault-bend folding above a simple flat-ramp-flat fault with a ramp angle of 29°),(2) background sedimentation/aggradation (general basinwide sedimentation) and (3) diffusive erosion, transport and deposition. The maximum long-term slip is split into horizontal and vertical components. Black = flat-ramp-flat fault; dark gray = folded bedding layer; light gray = base level. See text for discussion.

rare (e.g. Ford et al., 1997) and for this reason, we use here a numerical modelling approach to investigate possible growth strata geometries associated with fault-bend folds in three dimensions. An important issue in this kind of combined structural–stratigraphic modelling is that all simulated processes are manipulated simultaneously in order to realistically approximate the growth of real structures. Here, we use the methodology originally proposed by Waltham (1992) and applied to two-dimensional (2D) contractional structures by Hardy and Poblet (1995), and modify it to apply to 3D numerical modelling of fault-bend folding using kink-band kinematics (e.g. Suppe, 1983). We use a forward numerical modelling approach to investigate the geometry of growth strata associated with fault-bend folds in response to variations in accommodation space along the growing structure in both submarine and subaerial settings.

2. Numerical modelling methodology

2.1. Tectonic and sedimentary processes considered

Fig. 1 shows the tectonic and sedimentary processes considered in the modelling presented here: (1) tectonic deformation, (2) background sedimentation, and (3) local erosion, transport and deposition.

The tectonic process that we consider is the growth of a 3D fault-bend fold. The folding mechanism used is kink-band migration and, in particular, this study considers *parallel* fault-bend folding (e.g. Suppe, 1983) using a velocity description of deformation (Hardy and Poblet, 1995). Parallel fault-bend folding has been used by other authors in both basin-scale (Flemings and Jordan, 1990) and map-scale (Zoetemeijer et al., 1992, 1993) modelling. The more simple numerical implementation of *similar* fault-bend folding has led some authors to use it as an alternative (e.g. Chalaron et al.,1996; Bezemer et al., 1999). Although the applicability of Suppe's (1983) fault-bend fold model has been questioned (Ramsay, 1991), many authors have considered fault-bend folding and fault-related folding theories as good geometrical approximations of natural deformation in the upper crust (e.g. Jamison, 1987; Hardy and Poblet, 1995). In this study, the 3D structural geometry considered is a symmetric, doubly-plunging anticline; maximum long-term slip is in the central portion of the structure with a linear decrease to zero towards the lateral boundaries. Maximum long-term slip rates reported in the literature vary from 0.0 to 3.0 m/ka — these values encompassing both fault-bend folds (Hardy, 1994) and thrust faults in general (e.g. Flemings and Jordan, 1990; Leeder, 1999).

Background sedimentation represents general, basin-wide sedimentation and here it is defined as constant

throughout space and time during the modelling. This parameter does not represent any particular sedimentary process, but is used to model sedimentation in general (Hardy and Waltham, 1992; Waltham, 1992). Background sedimentation rates used in this study vary from 0.0 to 3.0 m/ka. Even though background sedimentation rates can be one or two orders of magnitude lower than tectonic rates (e.g. Suppe et al., 1991; Hardy, 1994; Leeder, 1999), the same range of rates is used here for both processes in order to study a range of conditions and resultant geometries.

Any structural high (submarine high or subaerial ridge) may lead to local erosion, transport and sedimentation. To account for this process, we implement the diffusion equation in three dimensions in which the sediment flux is assumed to be proportional to local slope and directed down the slope (e.g. Kenyon and Turcotte, 1985). This approach has previously been used when modelling local erosion, transport and deposition in two dimensions (e.g. Hardy and Poblet, 1995). The diffusion coefficient and its value and characteristics (linear or non-linear) are difficult to assess. Published estimates of the diffusion coefficient vary from 9×10^{-4} m^2/a for arid fault scarps (Colman and Watson, 1983) to 5.6×10^5 m^2/a for a prograding delta (Kenyon and Turcotte, 1985). Assuming erosion, transport and sedimentation associated with fault-related folding has a value somewhere in between these extremes, we use a value of 3 m^2/a, which has proven to be successful in illustrating the distinctive features caused by the interaction of tectonic and sedimentation in this setting (e.g. Hardy and Poblet, 1995).

Base level in the modelling approach represents a reference level above which there is no sedimentation. In marine environments, base level could represent, for example, the sea or wavebase level. In subaerial environments, base level may be controlled by a number of factors, but here we consider it to be the level to which sediments can aggrade. This parameter controls, together with tectonic uplift, the accommodation space in the system.

2.2. Numerical modelling approach

This study considers regional-scale structures: tectonic activity is confined to an area of 100 km^2 and the stratigraphic geometry of syn-tectonic sediments is studied within an area of 400 km^2 (Fig. 1). The modelling of sedimentary and tectonic processes is done using the general tectono–stratigraphic forward modelling equation proposed by Waltham (1992). This is a partial differential equation describing processes in terms of Eulerian variables, allowing structure and stratigraphy to be simulated as simultaneous rather than sequential processes.

The modelling approach used is based upon the concept that the height of a geological surface can be modified in four ways: (1) material can be added to, or removed from, the surface; (2) material can be moved from one part of the surface to another; (3) the surface can be moved; and (4) the surface can be deformed. The first two of these mechanisms are sedimentary, whereas the second two are tectonic (Waltham, 1992). The tectono–stratigraphic forward modelling equation used in this study is:

$$\frac{\partial h}{\partial t} = (p + \nabla \bullet F) + (Vz - \nabla \bullet [V(x,y) \times h]), \quad (1)$$

where ∂ = symbol indicating partial derivation, h = height of the geological surface at a fixed horizontal position (m), t = time (years), p = background sedimentation (m/year), F = sedimentary flux (m^2/year), V = velocity of tectonic deformation (m/year), x,y = horizontal coordinates (m), z = vertical coordinate (m), and $\nabla \bullet$ = Laplacian operator in Cartesian coordinates.

The first two terms of Eq. (1) represent sedimentary processes, whereas the second two terms represent tectonic processes. The maximum long-term slip is split into horizontal ($V(x,y)$) and vertical components (Vz) in order to achieve the velocity description of deformation for fault-bend folding (Hardy and Poblet, 1995; Waltham and Hardy, 1995), which is necessary to solve the tectono–stratigraphic forward modelling equation. The sedimentary flux (m^2/year) is assumed to be proportional to local slope, which gives the following expression for the diffusion equation:

$$\nabla \bullet F = -\alpha \nabla^2 h(x,y), \quad (2)$$

where α represents the diffusion coefficient.

The partial differential equation is discretized using a finite-difference approximation and the algebraic equations are solved using the *hopscotch* method, an explicit finite-difference scheme proposed by Gourlay (1970). The mesh dimension used in this study is 50×50 m^2. Modelling of tectonic and sedimentary processes using the tectono–stratigraphic forward modelling equation has previously proven to be successful when applied to regional-scale structures in two dimensions (e.g. Hardy, 1994; Hardy and Poblet, 1995; Ford et al., 1997). Here we show its application to 3D fault-bend folds.

3. Modelling a doubly-plunging fault-bend fold

We firstly model a simple doubly-plunging fault-bend fold without growth strata. The ramp dips at 29° and steps up from a flat décollement to an upper flat. The ramp height is 2250 m. The total model run time used is 1050 ka, with displacement varying between 0 and 3 m/ka from the edges to the centre of the structure, respectively, displacement being perpendicular to the strike of the fault. Thus, the tectonic component of this model is pseudo-3D (cf. Wilkerson et al., 1991). Two pre-tectonic horizons are included in the models to be used as geometric references.

A plan view of the upper pre-tectonic horizon, after deformation using the above parameters, is presented in Fig. 2. The transport direction is from left to right. In this figure,

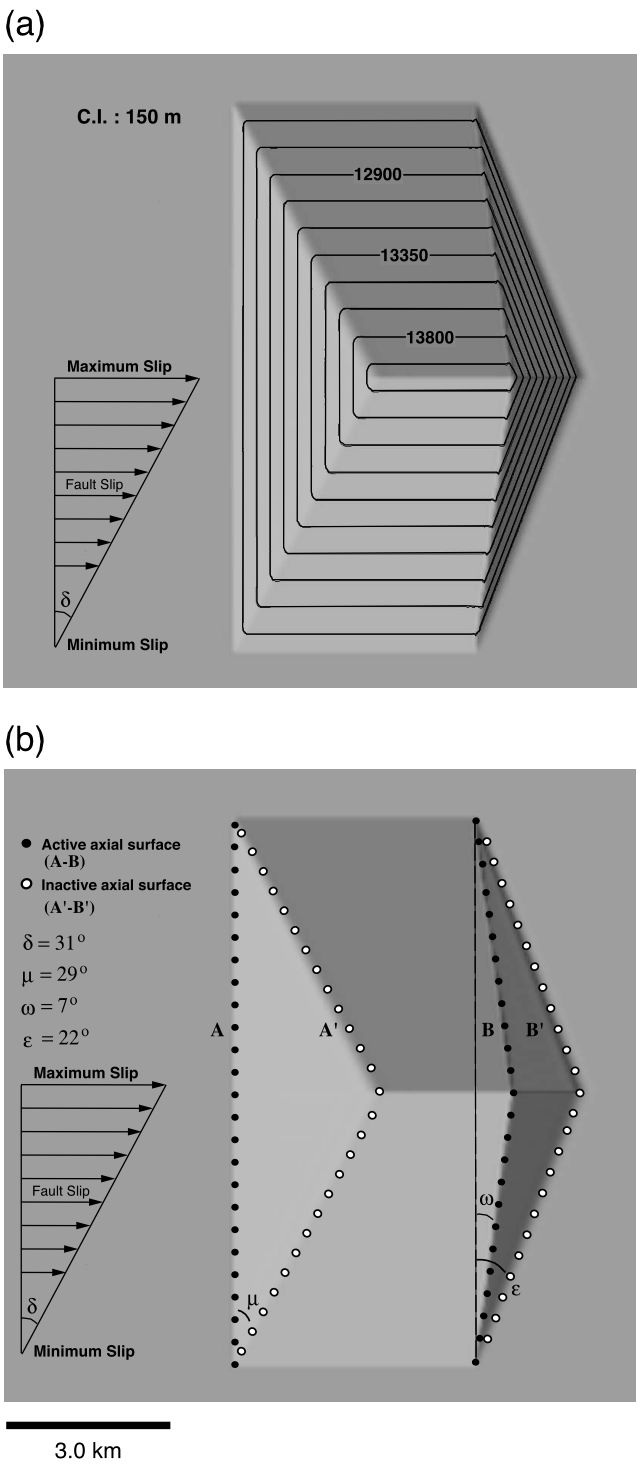

Fig. 2. Plan view of the upper pre-tectonic horizon after deformation. The transport direction is from left to right. The (a) structure contours and (b) 3D geometry of axial surfaces are in agreement with those proposed by Wilkerson et al. (1991) and Shaw et al. (1994) for a symmetric doubly-plunging parallel fault-bend fold. Illustrated slip gradient is symmetrically distributed about the centre of the structure. Angle notations taken from Wilkerson et al. (1991). See text for discussion.

structure contours of the horizon and the location of active (solid dots) and inactive (white dots) axial surfaces are shown. It can be observed that the geometry of the pre-tectonic horizon reflects the doubly-plunging geometry originally defined. The structure contours and the 3D geometry of axial surfaces observed in the anticline (Fig. 2a and b) are in exact agreement with those proposed by Wilkerson et al. (1991) and Shaw et al. (1994) for a symmetric, doubly-plunging fault-bend fold. The angle between the map traces of backlimb active and inactive axial surfaces (μ) is equal to 29° (Fig. 2b). The angles between a line parallel to the strike direction and the forelimb active (ω) and inactive axial surfaces (ϵ) are 7 and 22°, respectively. Considering the pseudo-3D approach proposed by Wilkerson et al. (1991), these values of μ and ϵ define a ramp of approximately 29°, which is in agreement with the value used in our modelling.

The along-strike displacement gradient, given as an angle δ (see Fig. 2a and b), for the values used in our modelling ranges from 0 to 30°. Empirical measurements of differential transport angles (δ) for continuous thrust sheets from different North American fold-thrust belts yield angles that do not exceed 35–40° without formation of tear faults (Wilkerson, 1992). The limit for transport angles observed in nature indicates that the range of differential transport angles used in our modelling represents natural structures properly.

For a doubly-plunging fault-bend fold, three-dimensional modelling using the velocity description of deformation presented here is clearly equivalent to structural-trend analysis by axial-surface mapping (Vertical Projection Method, Shaw et al., 1994), and the pseudo-3D approach proposed by Wilkerson et al. (1991). Although it is not shown here, we believe that this equivalence will be maintained if other changes along-strike are defined (e.g. changes in ramp dip or position of upper décollement). In this contribution, however, we additionally investigate the 3D geometry of syn-tectonic sediments associated with a doubly-plunging fault-bend fold.

4. Geometries of growth strata associated with a doubly-plunging fault-bend fold

We now consider the possible geometries of growth strata associated with the doubly-plunging fault-bend fold. In order to simulate natural growth structures, two stratigraphic models are considered. In both cases, the geometry of the fault and distribution of velocities are the same as those described in Section 3. The first model has been named the *submarine model* and represents a first approximation to structures developing in submarine environments. In this model, base level rise is equal to the maximum long-term slip rate, which allows the possibility of bathymetry to develop over the fault-bend fold. Bathymetry can arise in this situation because the vertical uplift rate, in the region of

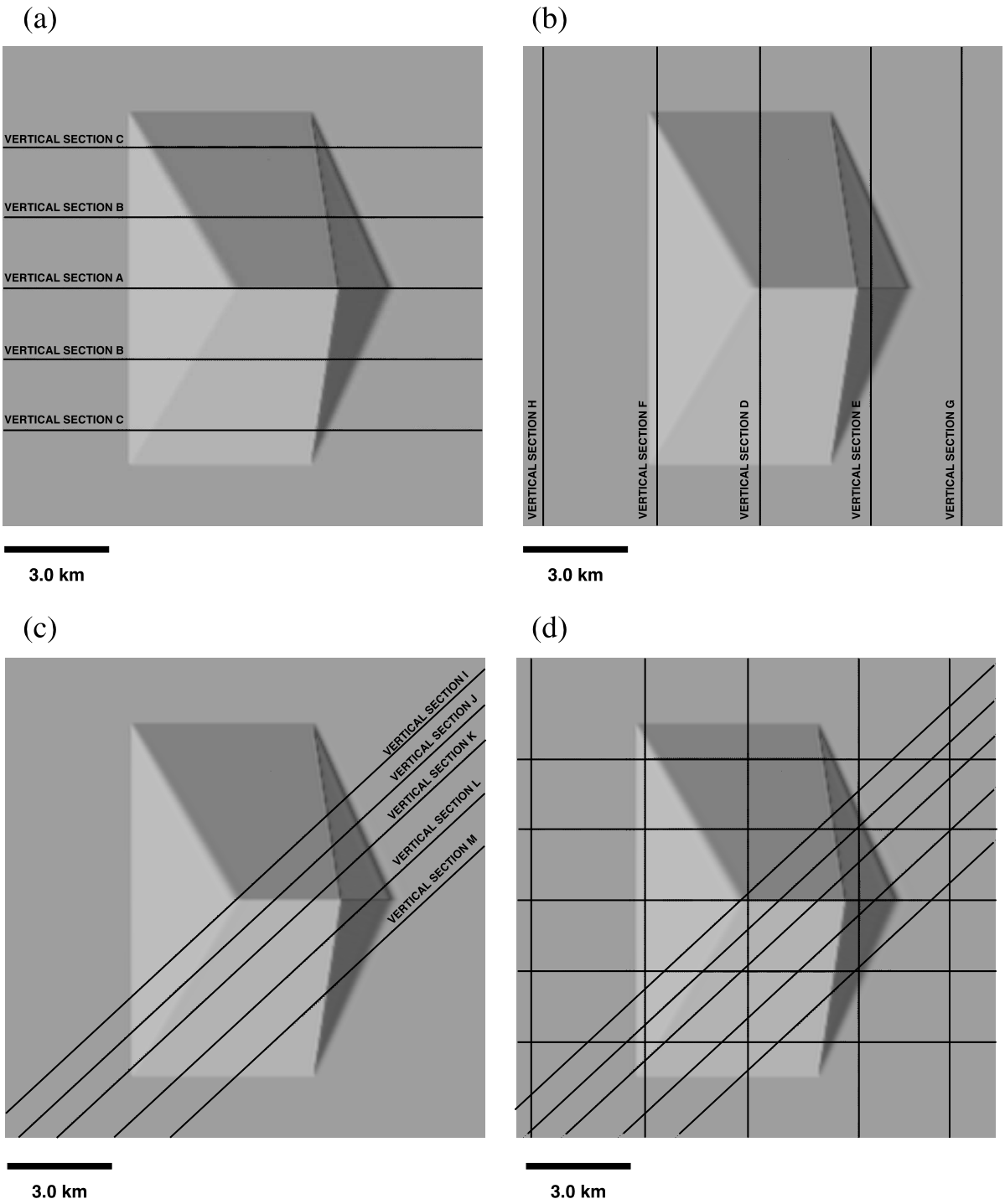

Fig. 3. Vertical sections used in this study. (a) Vertical sections in the plane of the transport direction (dip sections). (b) Vertical sections in the plane perpendicular to the transport direction (strike sections). (c) Vertical sections at a 45° angle to the transport direction (oblique sections). (d) The set of all vertical sections.

tectonic deformation, is lower than the maximum slip rate applied at the trailing edge (Hardy, 1995). The second model has been named the *subaerial model* and represents a first approximation to structures developing in, for example, intermountain basins. In this model, the base level rise is equal to the background sedimentation rate, which guarantees that all the accommodation is filled and simple aggradation to this base level occurs. This situation might approximately simulate alluvial sedimentation in intermountain basins. We study the 3D geometry of the syn-tectonic strata associated with these models using a series of 2D vertical cross-sections (Fig. 3) that possess a variety of orientations with respect to the orientation of the structure.

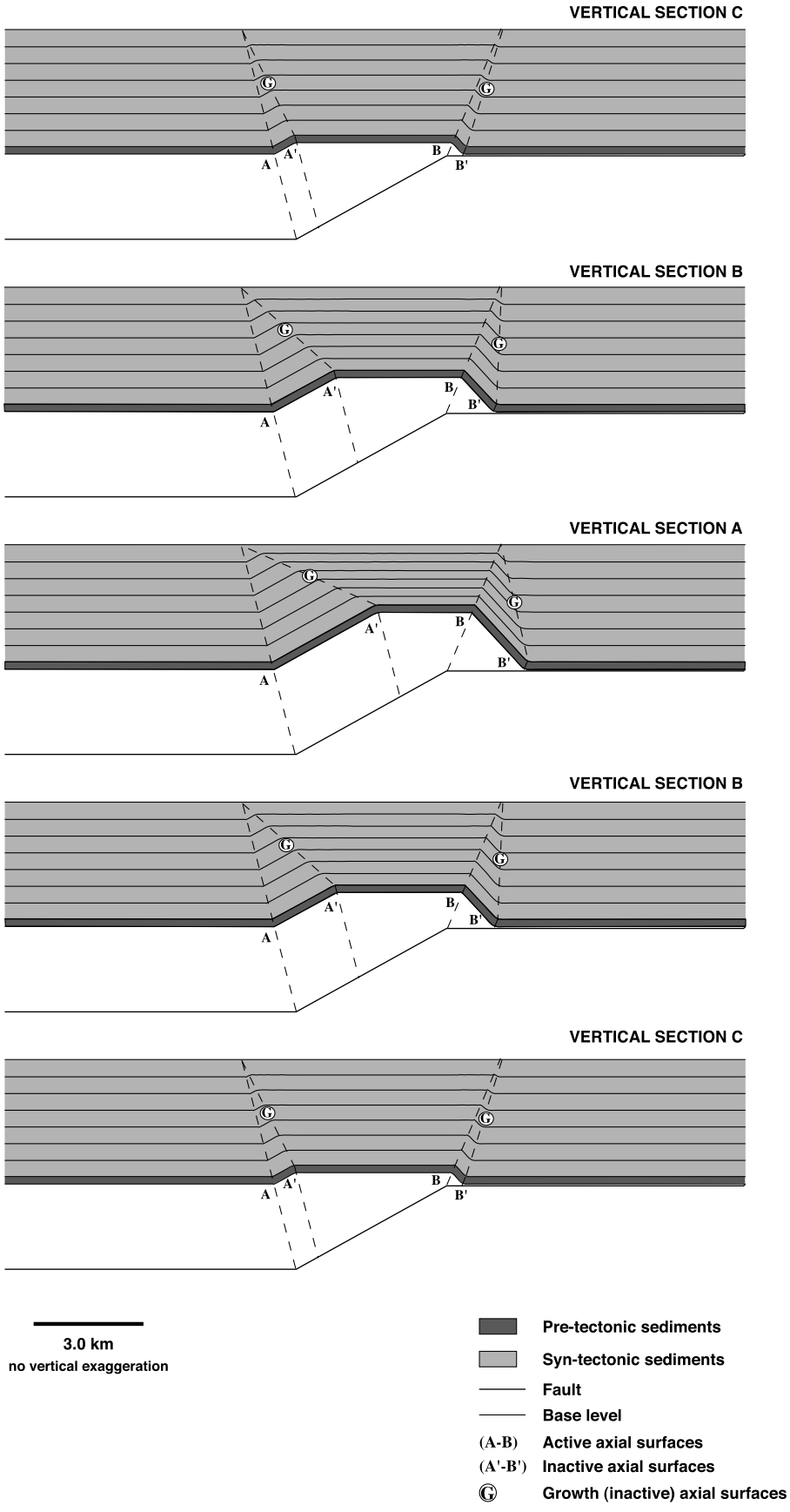
VERTICAL SECTION C
G
G
A
A'
B
B'
VERTICAL SECTION B
G
G
A'
B
B'
A
VERTICAL SECTION A
G
G
A'
B
B'
A
VERTICAL SECTION B
G
G
A'
B
B'
A
VERTICAL SECTION C
G
G
A
A'
B
B'
3.0 km
no vertical exaggeration
Pre-tectonic sediments
Syn-tectonic sediments
Fault
Base level
(A-B) Active axial surfaces
(A'-B') Inactive axial surfaces
G Growth (inactive) axial surfaces

Fig. 4.

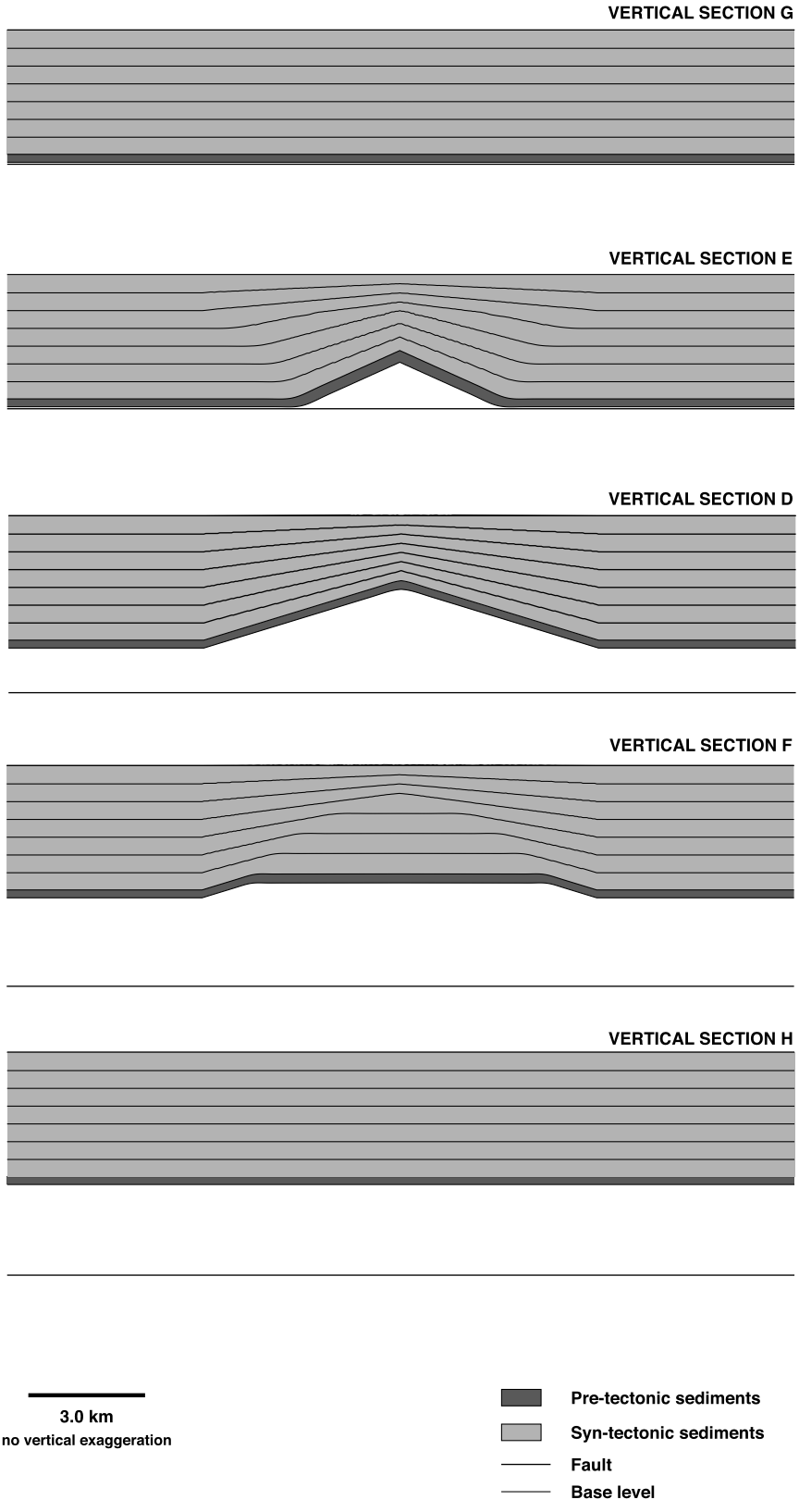

Fig. 4. (*continued*)

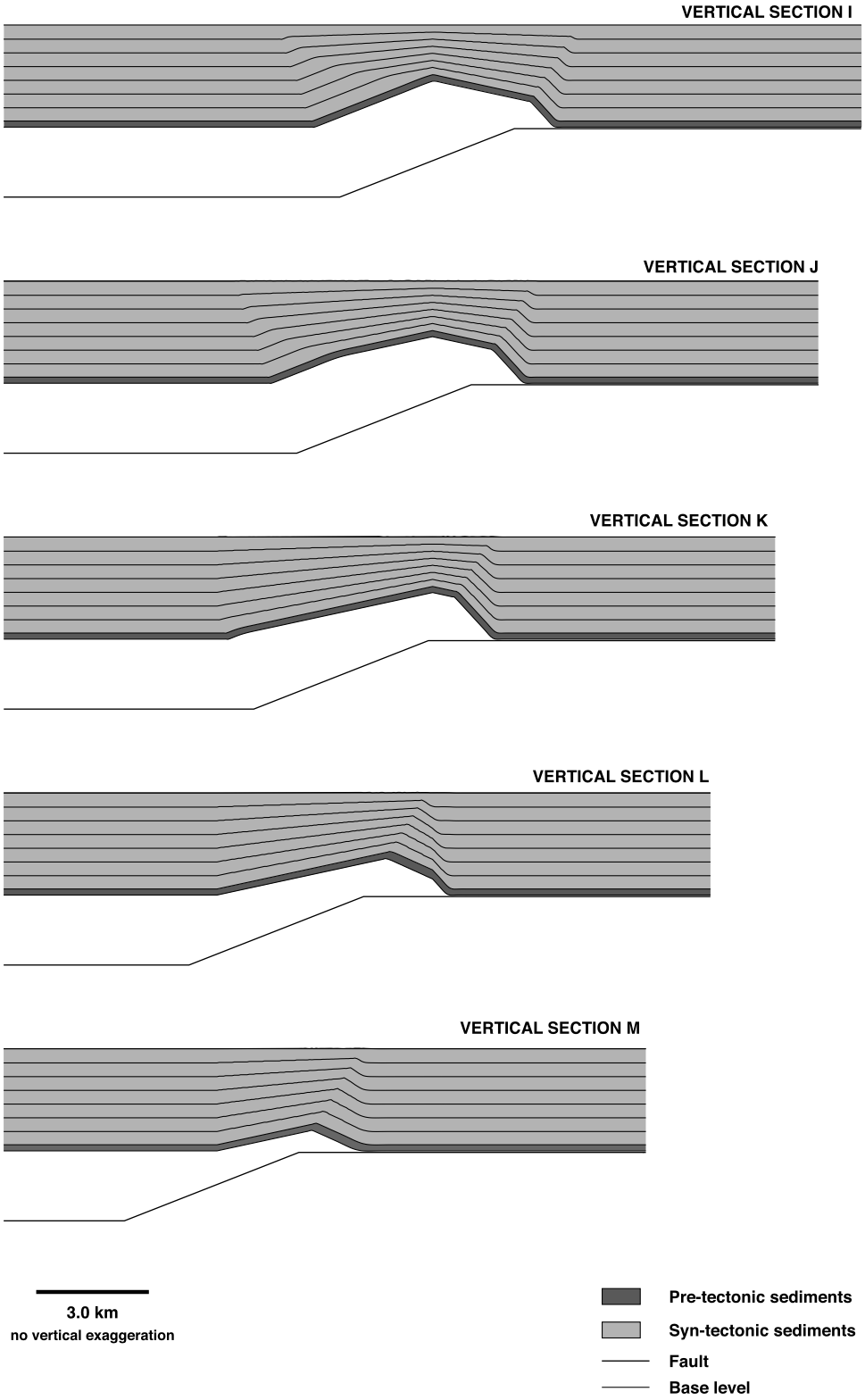

Fig. 4. Submarine model with background sedimentation of 3.0 m/ka, maximum slip rate of 3.0 m/ka, and diffusion coefficient of 0.0 m^2/ka. Growth strata are recorded at 150 ka intervals. (a) Vertical sections in the plane of the transport direction (dip sections). (b) Vertical sections in the plane perpendicular to the transport direction (strike sections). (c) Vertical sections at 45° to the transport direction (oblique sections).

4.1. Submarine model

In the *submarine model*, the geometry of syn-tectonic sediments will be studied under a variety of conditions. We will first consider the situation where no bathymetry develops above the developing structure and then consider the effects of (1) bathymetry and (2) local erosion, transport and deposition in the region of submarine highs.

Fig. 4a displays a series of vertical sections in the plane of the transport direction (dip sections) for a model where the base level was defined to start at the level of the top pre-tectonic horizon and to rise at a constant rate equivalent to the maximum slip rate. Rates of background sedimentation and maximum slip used in this model are 3.0 and 3.0 m/ka, respectively, producing a 'fill-to-the-top' geometry. The first two (lower) horizons represent pre-tectonic sedimentation and these are overlain by seven horizons representing syn-tectonic sedimentation recorded every 150 ka. Fig. 4b and c displays vertical sections in planes perpendicular (strike sections) and oblique to the transport direction, respectively, for the same model.

Pre-tectonic sediments in sections A, B and C (Fig. 4a) show growth by kink-band migration with differences in kink-band width between dip sections reflecting differences in total slip. Syn-tectonic sediments show thickness changes across the anticline and upward-narrowing growth triangles in both limbs. An active axial surface to the left and a growth axial surface to the right limit each growth triangle in all sections (Fig. 4a). The active axial surfaces represent the zone where sediments are folded and fractured, and they bisect the angle between dip panels in a parallel fault-bend fold (Suppe, 1983). In contrast, the growth axial surfaces represent the place where the rate of syn-tectonic sedimentation changes, and their geometry depends on all the parameters controlling accommodation space over the growing fault-bend fold. Sediment thicknesses to the left and right of growth axial surfaces are constant; therefore, the change in sedimentation rate observed in along-dip sections is abrupt. All the features presented above already have been described in previous modelling studies (Hardy, 1994; Hardy and Poblet, 1995) and compare very well with the models proposed by Suppe et al. (1991) and Shaw et al. (1994).

The width of the growth triangle and the orientation of the growth axial surfaces are different between the various dip sections. In section A (Fig. 4a), the widths of both backlimb and forelimb growth triangles are greater than the widths of those in section B, reflecting the greater total slip in this section. The same characteristic is observed between sections B and C. In section A, the change in sedimentation rate is also more evident than in sections B and C (Fig. 4a). In addition, both the backlimb and forelimb growth axial surfaces in section A rotate more toward the hinterland than those in section B. The same feature is observed between sections B and C.

Fig. 4b shows a series of vertical sections in the plane perpendicular to the transport direction (strike sections), an orientation not normally considered when examining growth strata. The transport direction is from bottom (section H) to top (section G) and the distribution of horizons representing pre- and syn-tectonic sedimentation is the same as that presented for the dip sections (see also Fig. 3). *Pre-tectonic* sediments in sections D (through the crest of the fault-bend fold) and E (through the forelimb) show a symmetric linear decrease (constant dip) of structural height from a maximum in the centre to zero at the boundaries. It is interesting to note that the geometry of pre-tectonic sediments in these sections resembles the geometry of pre-tectonic sediments associated with a symmetric detachment fold. Pre-tectonic sediments in section F (through the backlimb) also show a symmetric decrease (constant dip) of structural height from an upper plateau to zero at the boundaries. Pre-tectonic sediments in sections H and G show no deformation, as these sections are outside the zone of structural deformation (see Fig. 3). Sections D and E show noticeable thinning of *syn-tectonic* sediments along the structure towards the crest. Syn-tectonic sediments in these sections also decrease their dip from bottom (older) to top (younger) producing a fanning. Due to the location of section E with respect to the structure, growth strata do not display constant dip. In section F, the lower growth strata show a nonlinear decrease in height from a central planar region. In this planar region, the apparent thickness of syn-tectonic sediments is greater than that in any other zone over the structure, including the region of no tectonic activity, due to the obliquity of the section relative to the bedding dips. The upper growth strata show thinning along the structure towards the crest and a dip decrease from bottom to top (compare with section D). The change in structural position of the fault can be followed from the lower décollement (sections H and F) through the ramp (section D) to the upper décollement (sections E and G; Fig. 4b).

A series of oblique sections through the structure are shown in Fig. 4c. These sections are useful because they allow us to study structural and stratigraphic geometry considering dip and strike components simultaneously. Sections I–M represent sections at a 45° angle to the transport direction (see Fig. 3) from the centre (section I) to the edge (section M) of the structure. In these sections, *pre-tectonic* sediments exhibit a varying number of dip panels (Fig. 4c). The number of dip panels depends on the position of the oblique section with respect to the fault-bend fold. Oblique section I cuts through the backlimb, the upper plunging panel, and the forelimb producing three dip panels (see Fig. 3). In the same way, oblique section J cuts through the backlimb, upper and lower plunging panels, and the forelimb producing four dip panels. Oblique section M cuts through the lower plunging panel and the forelimb, and thus, shows only two dip panels. The geometry of the *syn-tectonic* sediments also depends on the position of the oblique section and varies markedly along strike. Growth

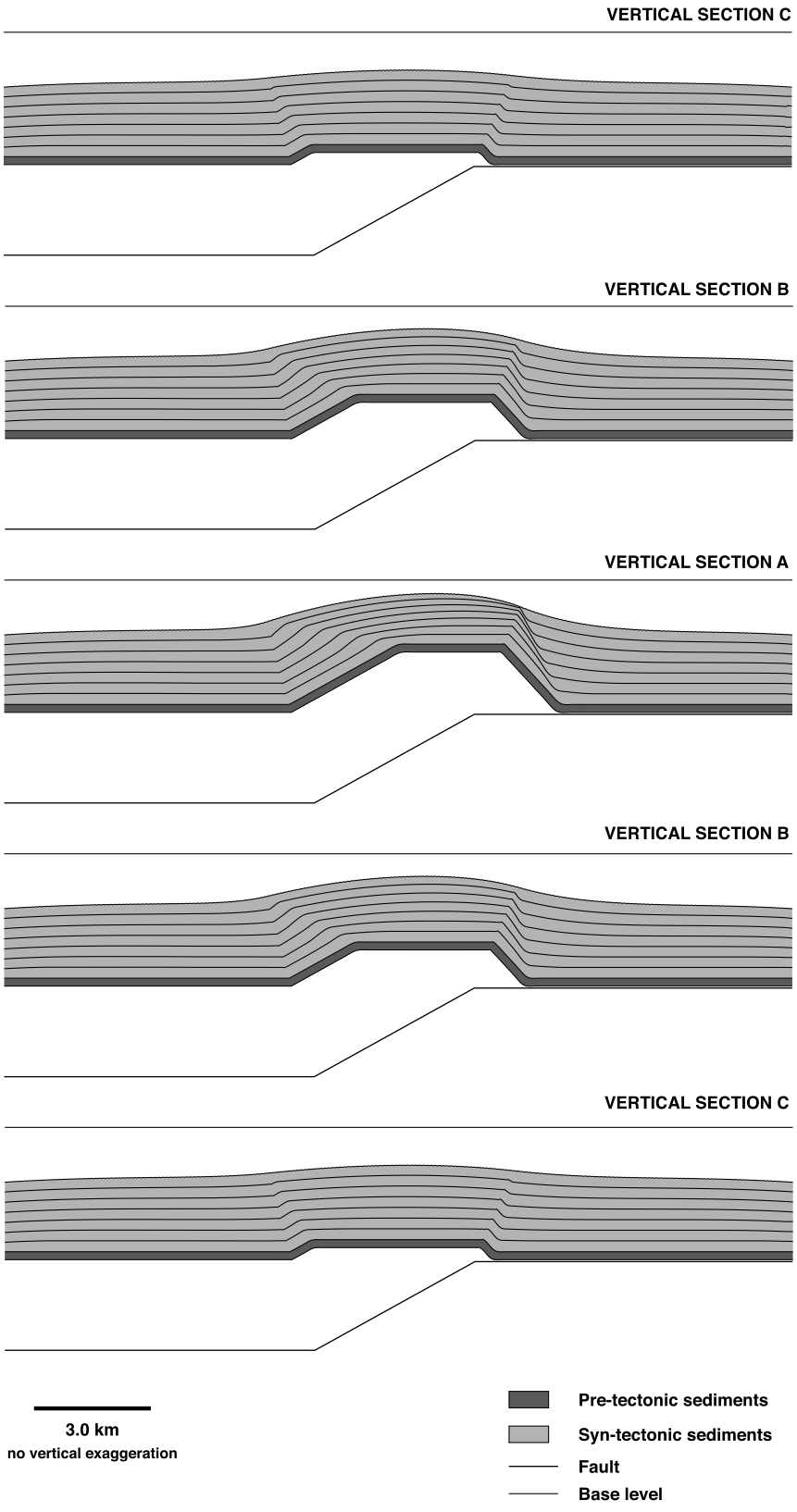

Fig. 5. Submarine model with background sedimentation of 1.8 m/ka, maximum slip rate of 3.0 m/ka, and diffusion coefficient of 3000.0 m^2/ka. Growth strata are recorded at 150 ka intervals. (a) Vertical sections in the plane of the transport direction (dip sections). (b) Vertical sections in the plane perpendicular to the transport direction (strike sections). (c) Vertical sections at 45° to the transport direction (oblique sections).

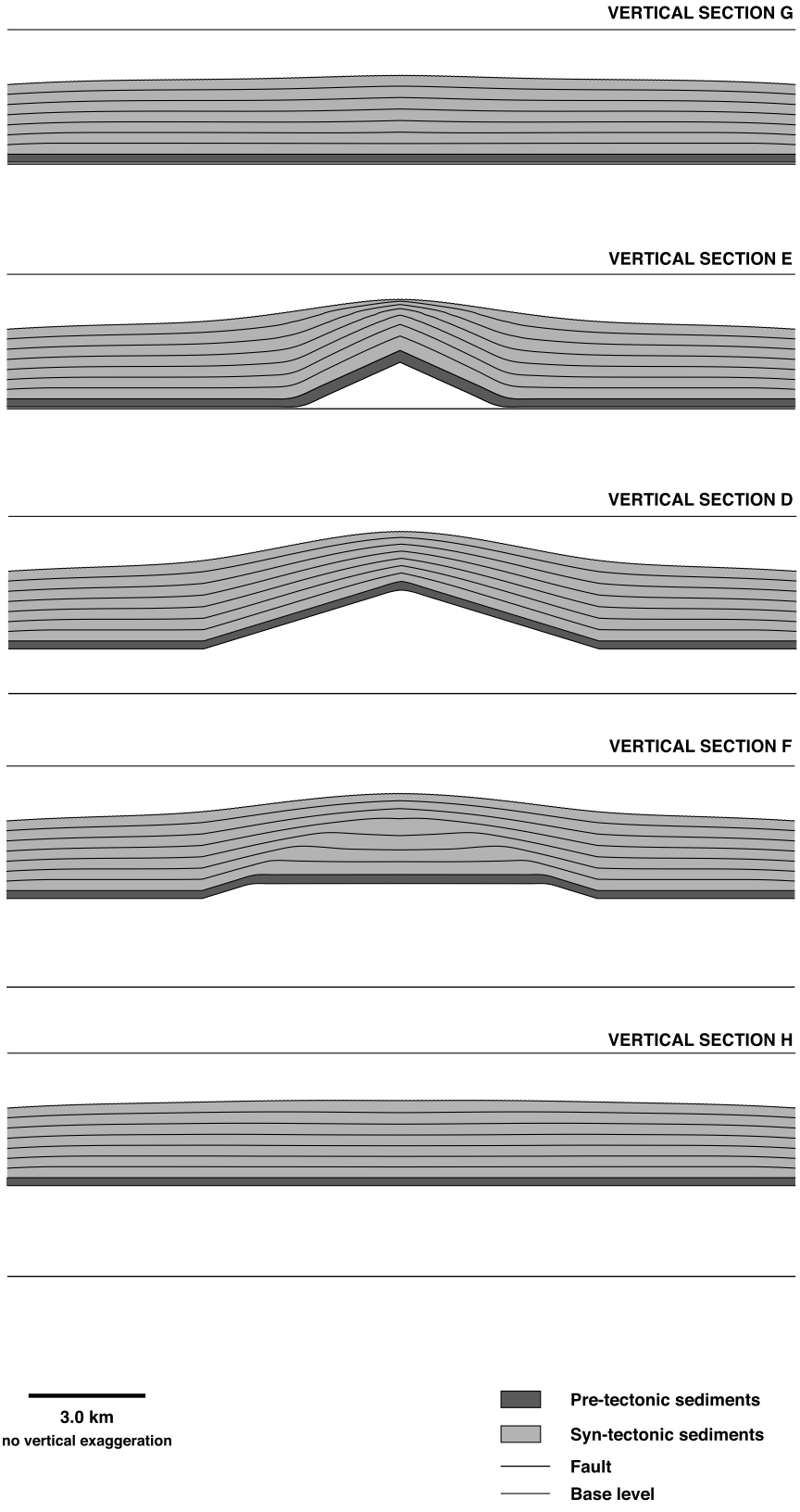

Fig. 5. (*continued*)

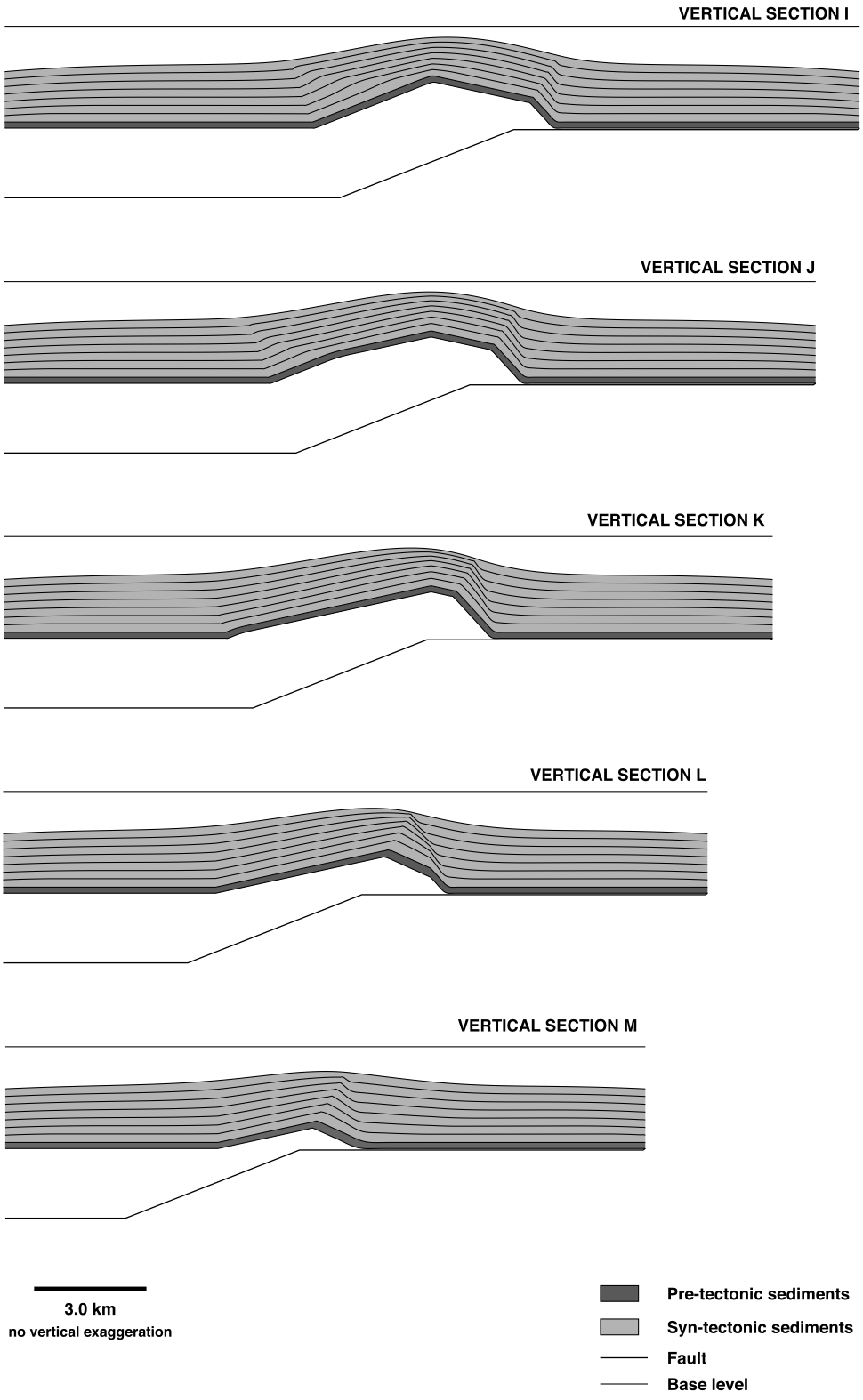

Fig. 5. (*continued*)

strata in sections I and J show backlimb and forelimb growth triangles, thinning across the crest of the structure and a dip decrease from bottom to top (fanning; Fig. 4c). Here we can see the manner in which the growth-strata geometries of both dip and strike sections are displayed in the oblique section. Oblique sections K, L, and M show forelimb growth triangles, thinning over the crest of the structure and fanning, but lack backlimb growth triangles. The geometries

present in the growth strata thus clearly depend not only on the amount of slip but also on the position of the oblique section (compare sections K and M).

There is no bathymetry in any of the sections described above (dip, oblique or strike) because the background sedimentation rate is high enough to fill all the accommodation space available, producing a 'fill-to-the-top' geometry. We now study the geometry of growth strata when bathymetry is allowed to develop across the structure. This is done by reducing the background sedimentation rate to 1.8 m/ka and including a diffusion coefficient of 3000 m^2/ka to simulate local erosion, transport and sedimentation (e.g. slumping). All other model parameters are the same as in Fig. 4.

A series of dip sections through this model are shown in Fig. 5a. In this set of dip sections, the attitude of backlimb and forelimb growth axial surfaces records differences in accommodation space in the same way as was explained for Fig. 4a. However, note the curved (smooth) morphology of syn-tectonic sediments over and outside the zone of structural deformation. This morphology is associated with the redistribution of material (diffusion) over the growing fault-bend fold. Compare the curved morphology of syn-tectonic sediments shown in Fig. 5a with the linear morphology displayed in Fig. 4a. Other features such as the width of growth triangles between sections are similar to those discussed for the 'fill-to-the-top' model.

Fig. 5b displays a series of strike sections for this model. All the sections show the smooth morphology already discussed for the dip sections. Sections D and E show thinning of syn-tectonic sediments towards the crest of the structure and fanning. These geometries are not as clear as those shown in Fig. 4b, but they can still be observed in Fig. 5b. Section F displays lower growth strata with three smoothly curving dip panels, whereas upper growth strata only show thinning over the crest and fanning.

A series of vertical sections in the plane oblique to the transport direction is shown in Fig. 5c. The curved morphology of syn-tectonic strata over and outside the region of structural deformation is a characteristic feature in all sections. Backlimb and forelimb growth triangles, thinning of syn-tectonic sediments over the crest and fanning are variably shown in these sections. These geometries are not as clear as those shown in Fig. 4c, but they are still discernible. Note once more the manner in which growth strata geometries change rapidly along-strike.

In order to emphasise the effect of local erosion, transport and deposition on growth strata geometries, the background sedimentation rate is reduced further to 0.55 m/ka. All other parameters are kept as in Fig. 5. Fig. 6a shows a series of dip sections for the set of parameters described above. The bathymetry developed over the anticline is clearly greater than that observed in Fig. 5a. Note how the backlimb and forelimb growth axial surfaces rotate toward the hinterland from section C to section A. Furthermore, in section A, these growth axial surfaces 'disappear' and they are replaced by a time-transgressive unconformity, such that syn-tectonic sediments lie below the unconformity in one region of the structure (offlap geometry in the backlimb) and above it in other regions of the structure (e.g. onlap geometry in the forelimb). The curved morphology of syn-tectonic sediments discussed in Fig. 5a is also observed in these sections.

A series of vertical sections in the plane perpendicular to the transport direction (strike sections) are displayed in Fig. 6b. Growth strata in section D display thinning over pre-tectonic sediments and fanning. These growth strata disappear over the crest of the fault-bend fold, showing an offlap configuration in this area. In contrast, in section E the lower syn-tectonic sediments onlap pre-tectonic sediments with later growth strata overlapping the structure. In section F, syn-tectonic sediments show fanning and then thinning over syn-tectonic sediments (Fig. 6b) until they disappear in the upper region of the backlimb.

Fig. 6c shows a series of oblique sections for the model described above. The configuration of the growth strata is now quite complex. Section I shows backlimb and forelimb growth triangles and syn-tectonic sediments thinning over pre-tectonic sediments until they disappear over the crest of the fault-bend fold. Growth strata in section J exhibit a backlimb growth triangle and thinning over the crest of the anticline, where they display an offlap configuration. Syn-tectonic sediments onlapping pre-tectonic sediments in the forelimb of the fault-bend fold are observed in sections K, L, and M (compare with Fig. 5c). Sections K and L show growth strata thinning over the backlimb until reaching an offlap configuration over the crest of the anticline (compare with sections K and L in Fig. 5c). Syn-tectonic sediments in section M exhibit a geometry similar to that presented in Fig. 5c.

4.2. Subaerial model

In the *subaerial model*, the geometry of syn-tectonic sediments is studied under a set of conditions similar to that of the *submarine model*. In order to simulate simple aggradation, sedimentation rate and base level rise are considered equal in the subaerial model. The model-run time, transport direction, distribution of pre- and syn-tectonic sediments and positions of vertical sections are the same as those presented for the *submarine model*. However, the values of aggradation used are different in order not to simply reproduce the stratal patterns of the *submarine* model. Rather than describe all the features of the subaerial model results, we will focus on the key differences between them and those of the submarine model.

We initially use rates of aggradation and maximum slip of 2.0 and 3.0 m/ka, respectively, to produce a 'fill-to-the-top' geometry. Fig. 7a shows vertical sections in the plane of the transport direction, whereas Fig. 7b and c shows strike and oblique sections, respectively. The geometries of syn-tectonic sediments are similar to those presented for the

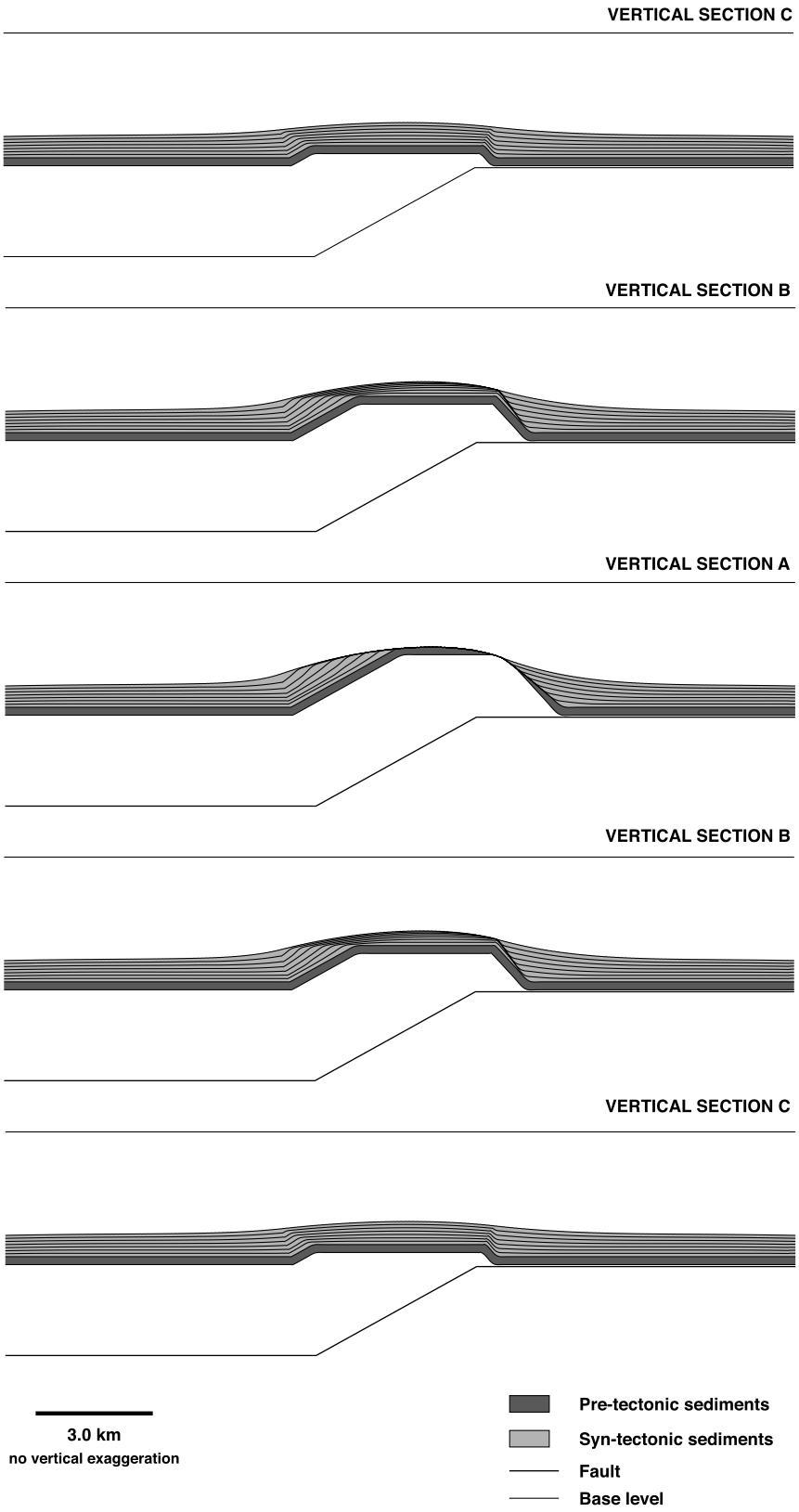

Fig. 6. Submarine model with background sedimentation of 0.55 m/ka, maximum slip rate of 3.0 m/ka, and diffusion coefficient of 3000.0 m^2/ka. Growth strata are recorded at 150 ka intervals. (a) Vertical sections in the plane of the transport direction (dip sections). (b) Vertical sections in the plane perpendicular to the transport direction (strike sections). (c) Vertical sections at 45° to the transport direction (oblique sections).

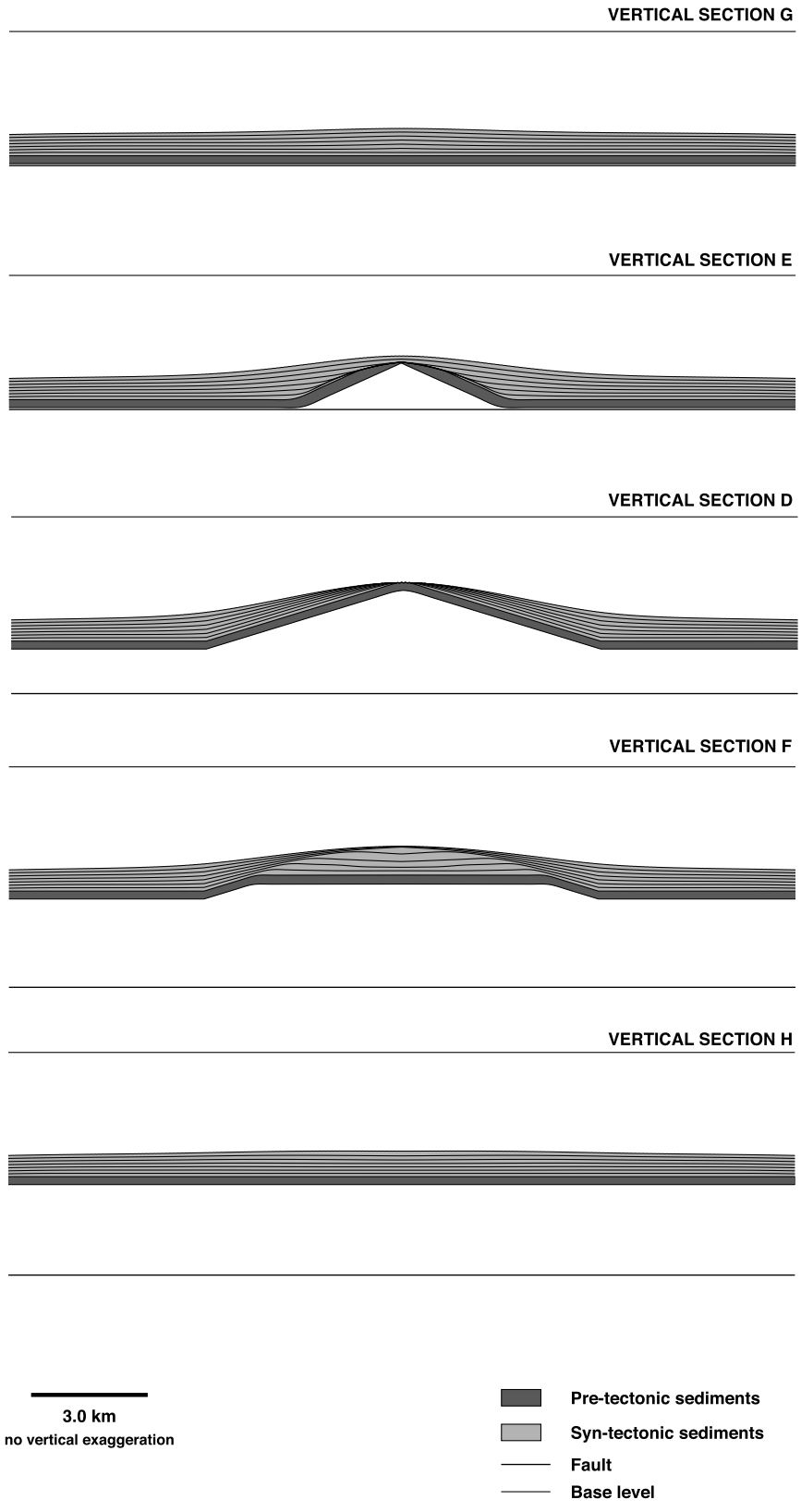

Fig. 6. (*continued*)

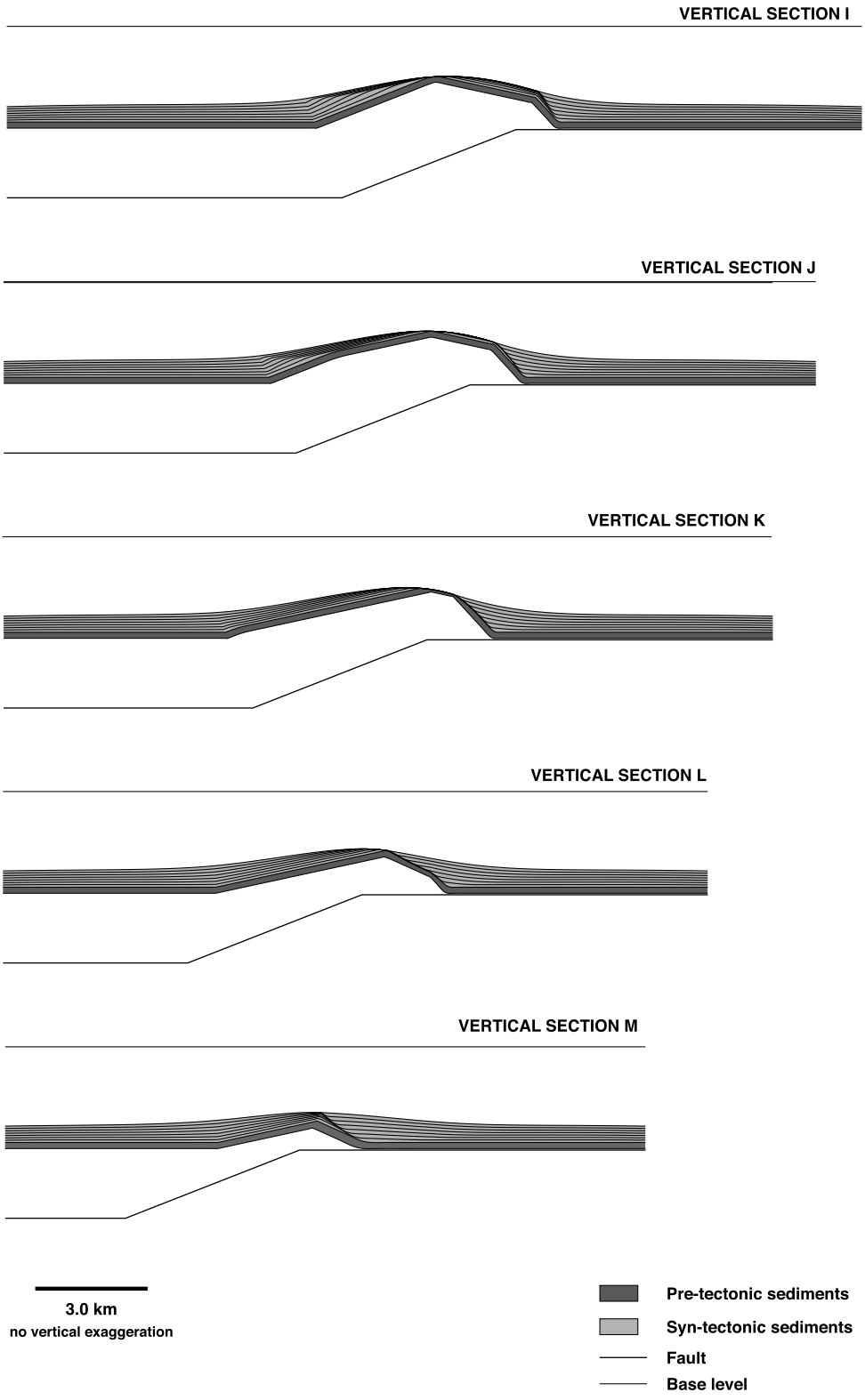

Fig. 6. (*continued*)

submarine case in the situation of 'fill-to-the-top' (compare Figs. 4 and 7), showing upward-narrowing growth triangles in both limbs, clear thinning of syn-tectonic sediments along the structure towards the crest, and fanning. As before, strike and oblique sections display complex structural and stratigraphic configurations reflecting the orientation of the sections with respect to the transport direction. The main effect of the lower aggradation rate in the subaerial model is

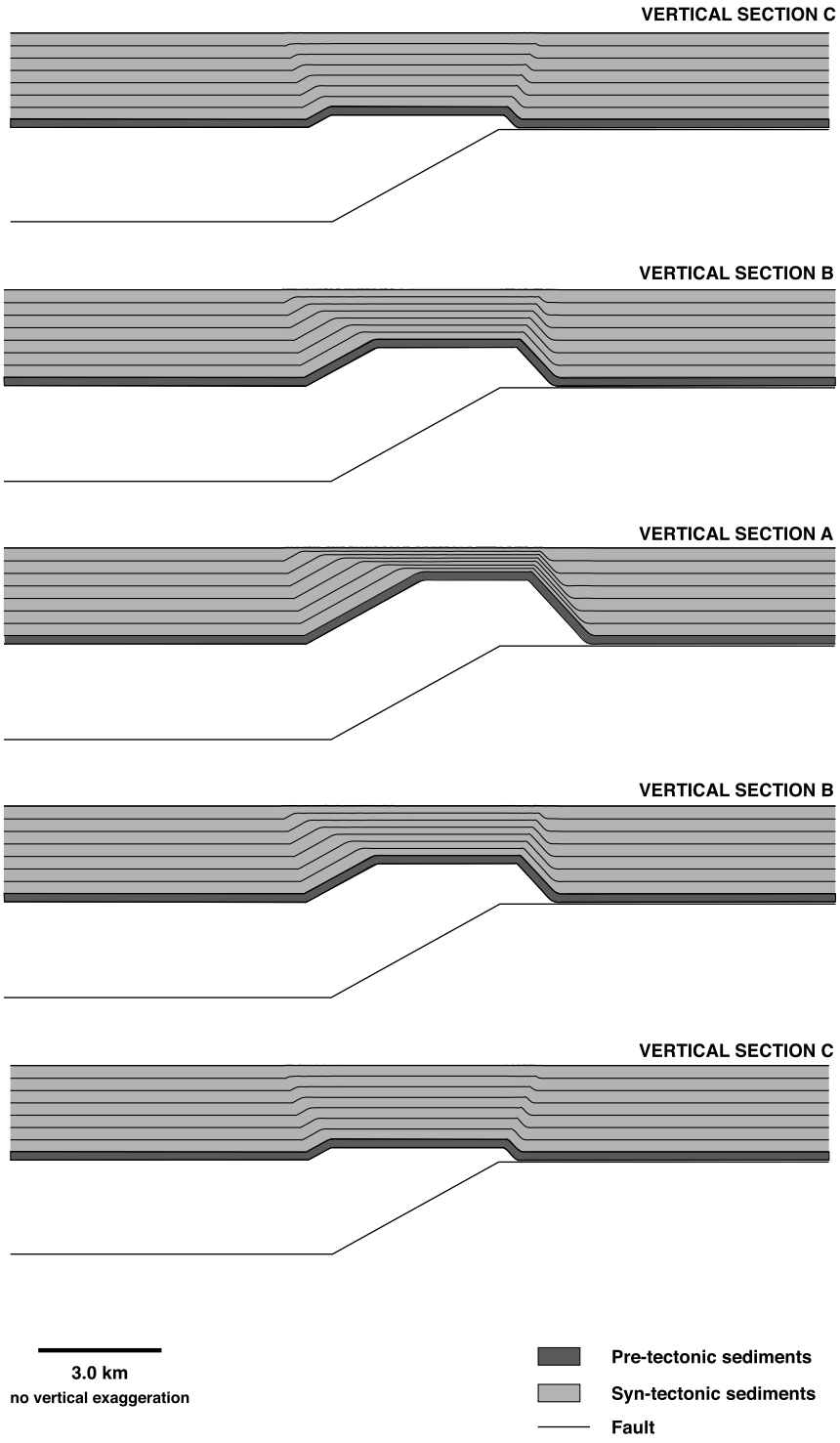

Fig. 7. Subaerial model with background sedimentation of 2.0 m/ka, maximum slip rate of 3.0 m/ka, and diffusion coefficient of 0.0 m^2/ka. Growth strata are recorded at 150 ka intervals. (a) Vertical sections in the plane of the transport direction (dip sections). (b) Vertical sections in the plane perpendicular to the transport direction (strike sections). (c) Vertical sections at 45° to the transport direction (oblique sections).

that inactive axial surfaces rotate more toward the hinterland than those of the equivalent submarine model (compare Figs. 4a and 7a).

We will now examine the geometry of growth strata when topography develops across the structure. This will be done by reducing the aggradation rate to 1.1 m/ka and including a diffusion coefficient of 3000 m^2/ka to simulate local erosion, transport and sedimentation. All other parameters are the same as in Fig. 7. Fig. 8a shows a series of vertical sections in the plane of the transport direction for the set of

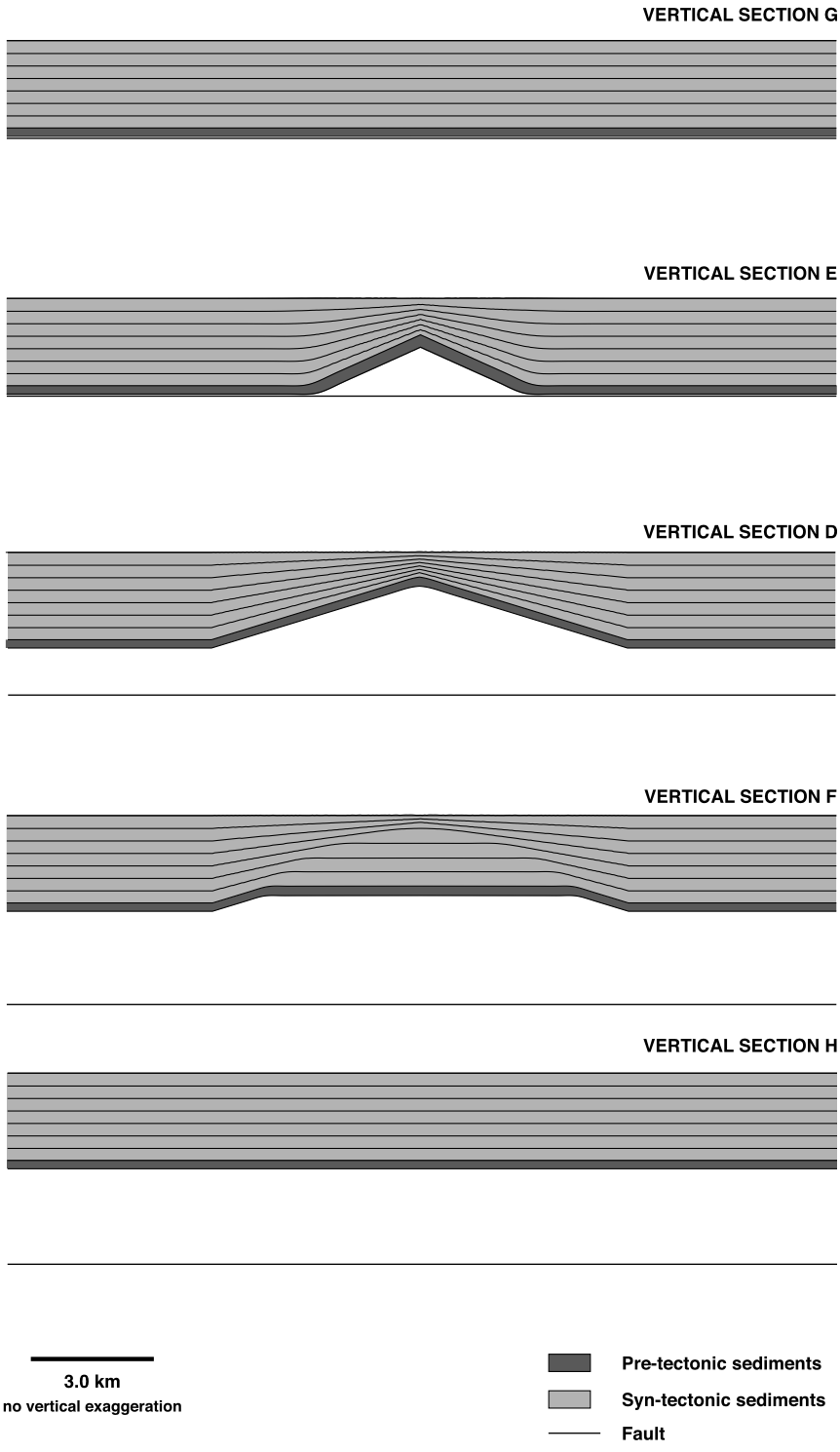

Fig. 7. (*continued*)

parameters considered above. The geometry of syn-tectonic sediments observed in Fig. 8a is similar to that observed in Fig. 7a, but now material in the region of maximum structural relief has been eroded and distributed over the growing anticline. The effect of erosion can be clearly seen in section A (compare Figs. 7a and 8a). Marked differences are also seen between this model and the equivalent submarine model where background sedimentation occurs across the entire structure (compare Figs. 5a and 8a). In the submarine model, growth strata thin across the crest of the structure in the region of maximum structural relief, but blanket pre-growth strata from erosion. In the subaerial case, the fact that no sedimentation occurs in this region allows deep erosion of the pre-growth strata (cf. Figs. 5a and 8a).

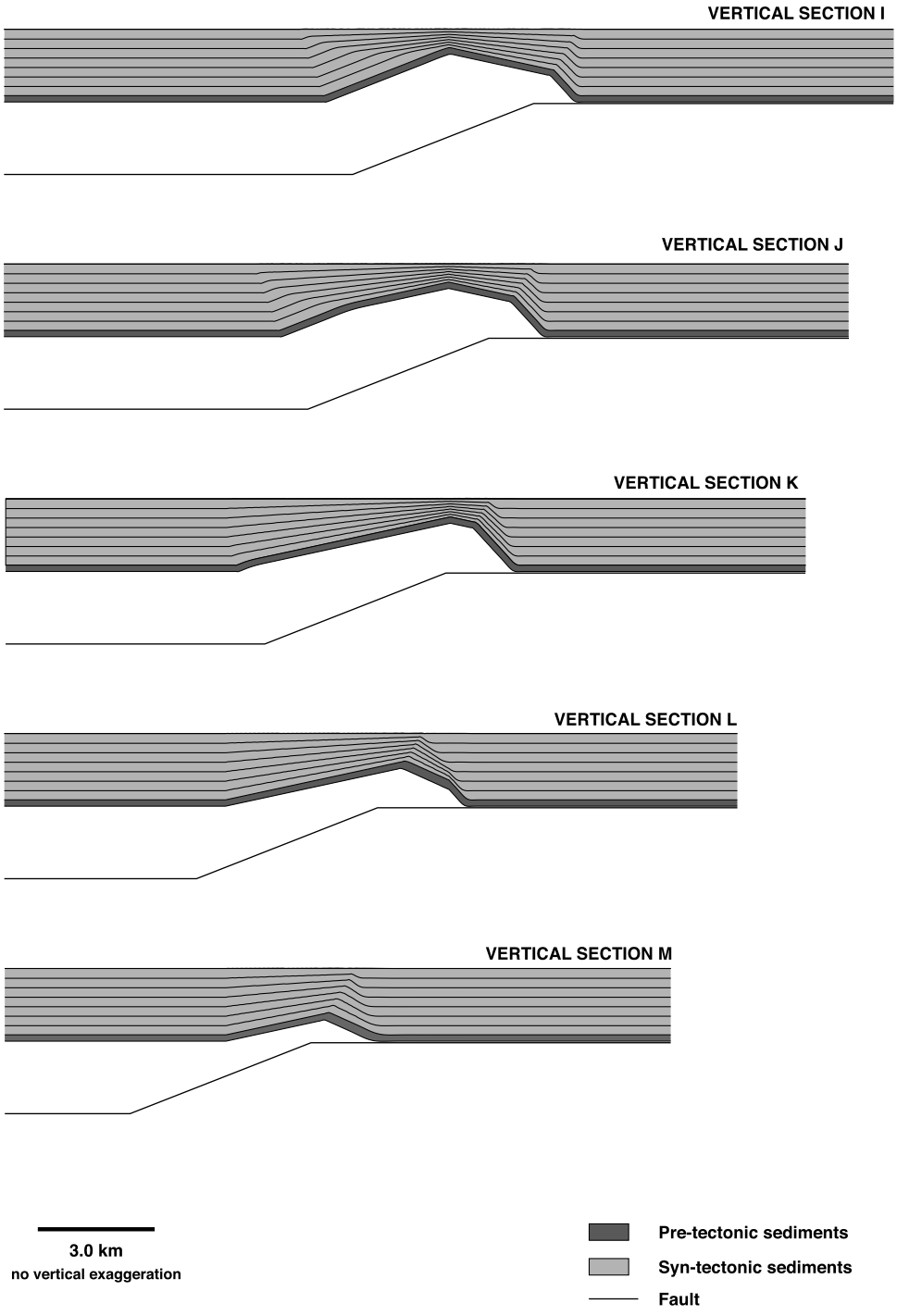

Fig. 7. (*continued*)

A set of vertical sections in the plane perpendicular to the transport direction is shown in Fig. 8b. Compared with the submarine sections shown in Fig. 5b, marked thinning and absence of growth strata in the region of maximum structural relief is once more seen. This is particularly apparent in Sections D and E, which show syn-tectonic sediments thinning over the limbs of the anticline and fanning and removal of material (pre- and syn-tectonic sediments) in the region of structural relief (compare with sections D and E in Fig. 5b). Oblique sections for this model show similar erosion and thinning over the region of maximum structural relief (Fig. 8c).

There is little structural relief in any of the vertical sections shown in Fig. 8 because of the relatively high aggradation rate and high diffusion coefficient. In order to simulate more realistic situations where a subaerial ridge develops, the background sedimentation (aggradation) rate is further reduced to 0.55 m/ka. All other parameters are

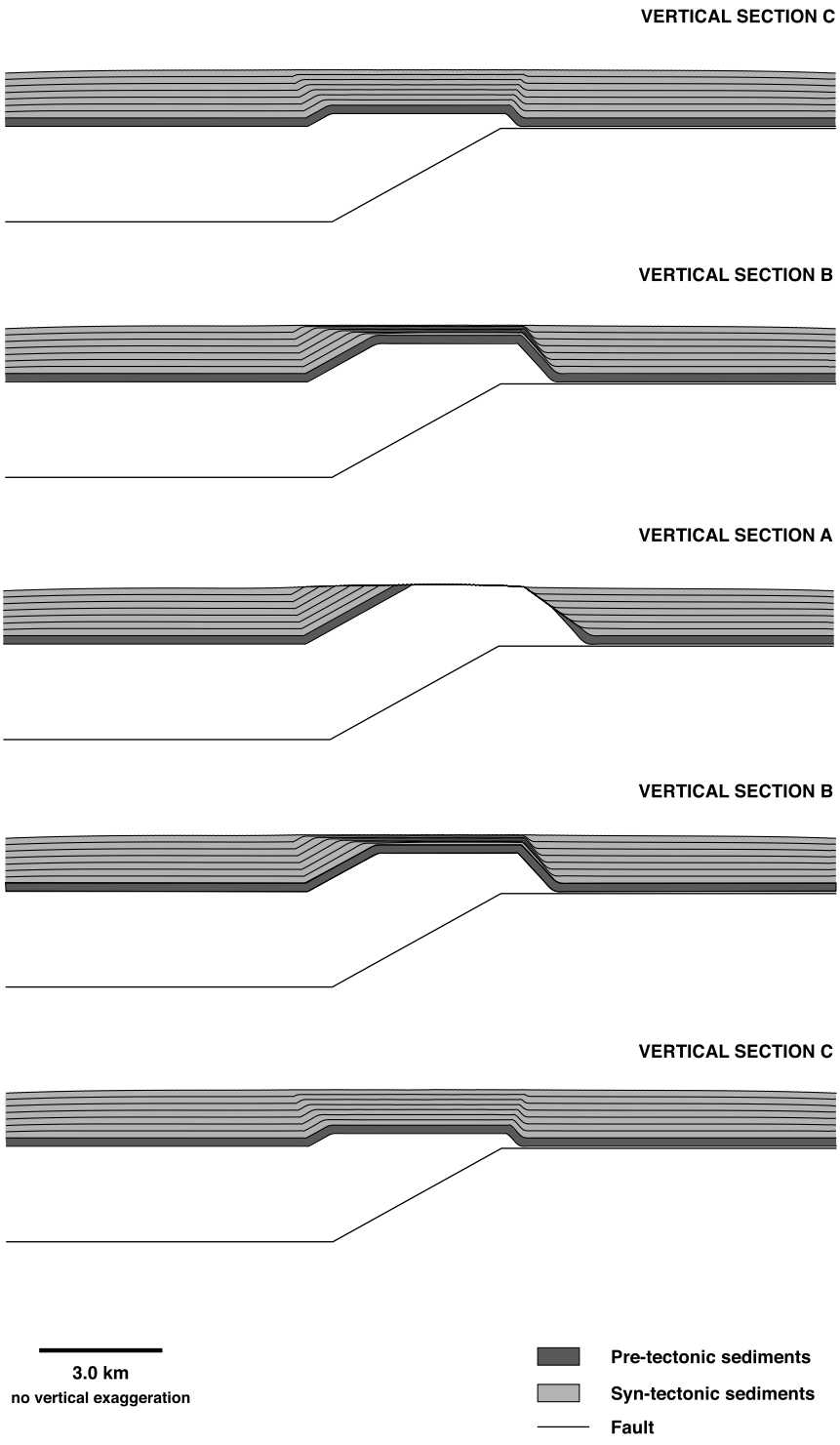

Fig. 8. Subaerial model with background sedimentation of 1.1 m/ka, maximum slip rate of 3.0 m/ka, and diffusion coefficient of 3000.0 m^2/ka. Growth strata are recorded at 150 ka intervals. (a) Vertical sections in the plane of the transport direction (dip sections). (b) Vertical sections in the plane perpendicular to the transport direction (strike sections). (c) Vertical sections at 45° to the transport direction (oblique sections).

kept as in Fig. 8. Fig. 9a shows a series of vertical sections in the plane of the transport direction for the set of parameters described above. Note how the backlimb and forelimb growth axial surfaces rotate toward the hinterland from section C to sections B and A. In sections A and B, these growth axial surfaces 'disappear', and they are replaced by a time-transgressive unconformity in the same way that was described for the *submarine model* in Fig. 6a. With the reduced aggradation rate, pronounced subaerial relief develops, particularly in sections A and B. A set of vertical sections in the plane perpendicular to the transport direction is shown in Fig. 9b. In section D, growth strata thin over the

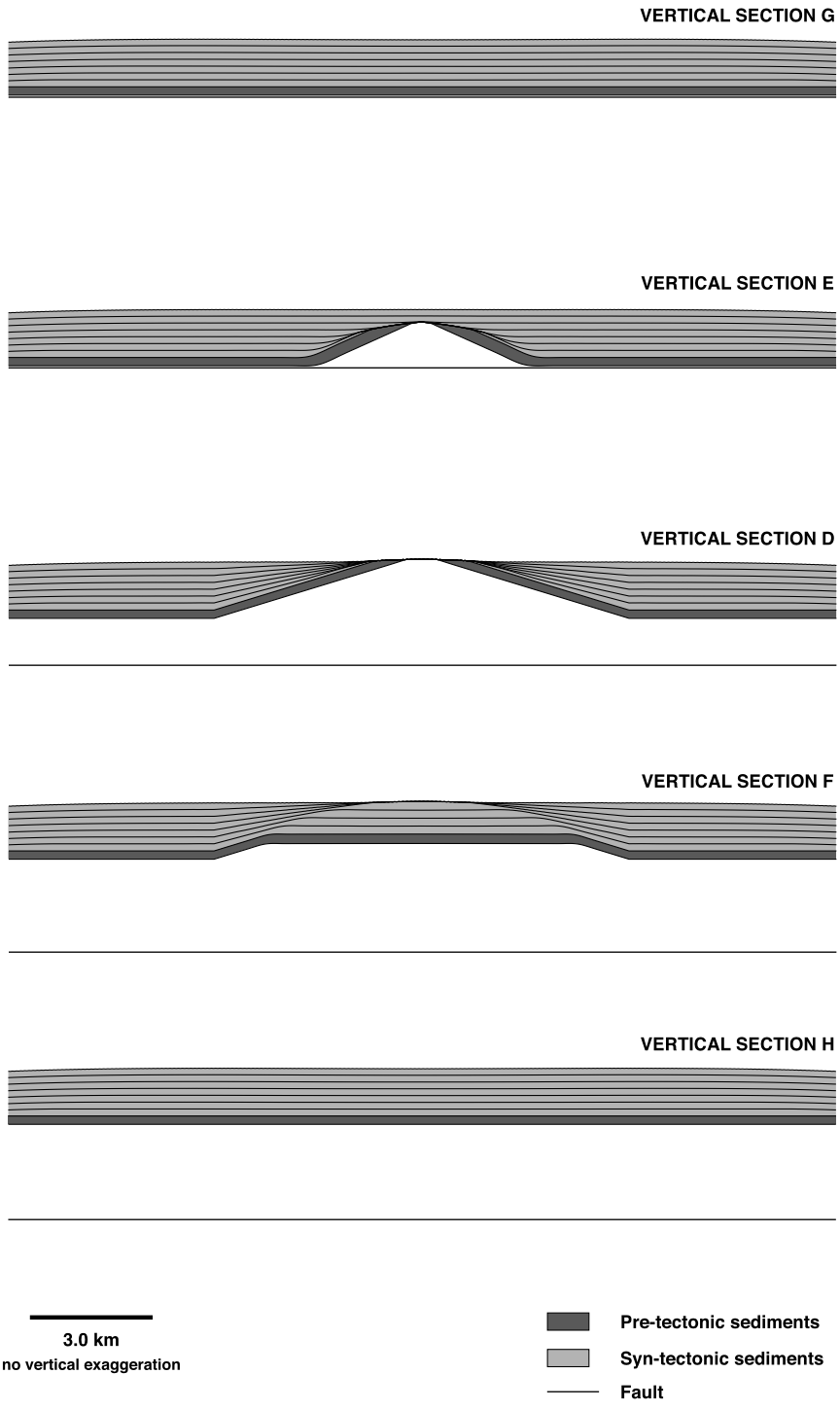

Fig. 8. (*continued*)

limbs of the anticline and show strong fanning. In contrast, in section E syn-tectonic sediments onlap and eventually overlap pre-tectonic sediments. Upper syn-tectonic sediments thin and fan over lower syn-tectonic sediments in section F. Fig. 9c displays a series of oblique sections through this model. In sections I and J, syn-tectonic sediments show an offlap geometry in the backlimb and onlap pre-tectonic sediment in the forelimb. In sections K, L, and M, syn-tectonic sediments thin and fan over the backlimb and onlap pre-tectonic sediments in the forelimb. Sections I, J, K, and L display erosion of material from the crest of the anticline. In all sections the main difference between this model and the equivalent submarine model is the deep erosion of the crest of the structure due to the lack of sedimentation in this region (compare Figs. 6 and 9).

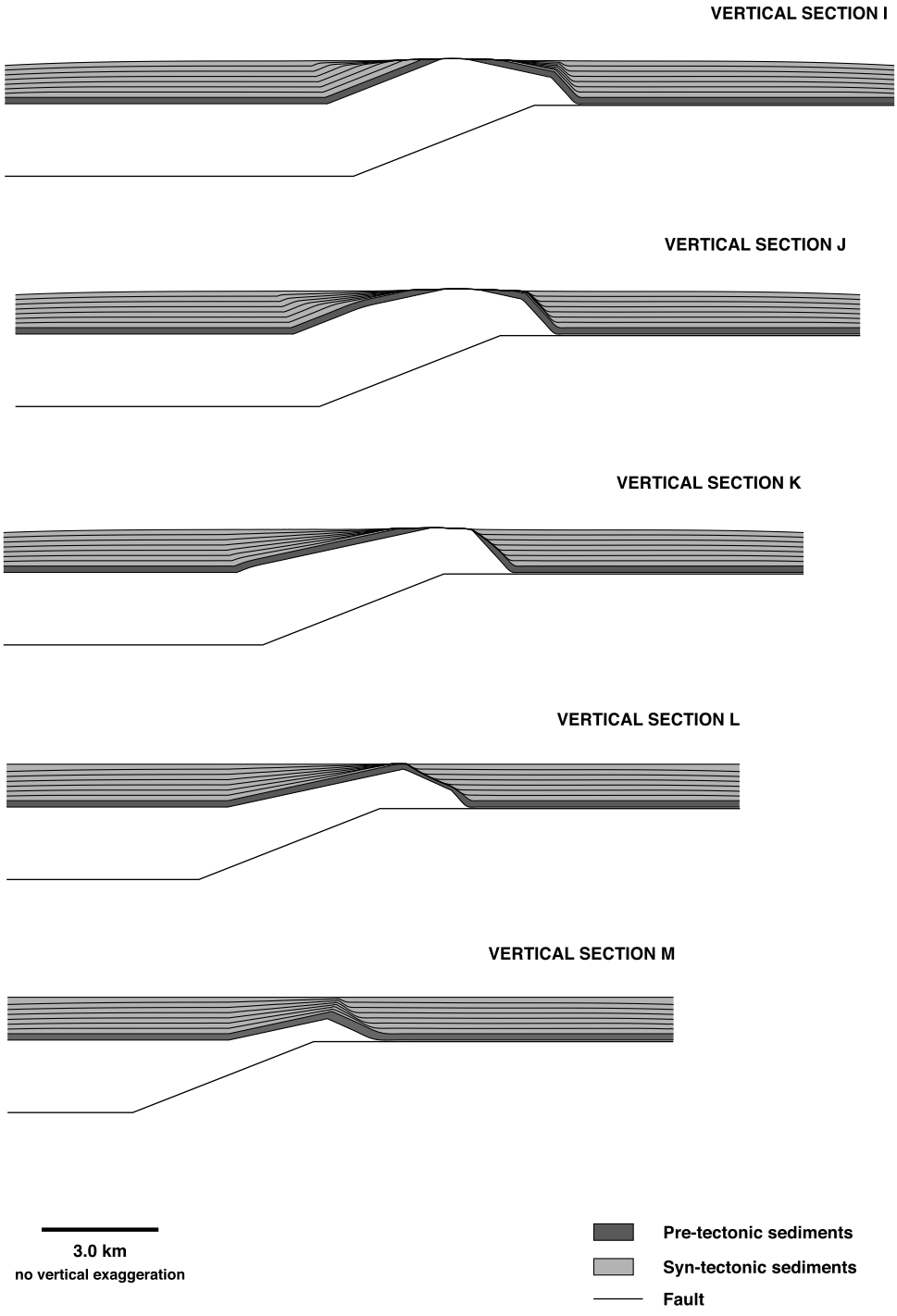

Fig. 8. (*continued*)

5. Discussion

The geometries displayed by both the subaerial and submarine models show some similarities and differences, and have implications for the interpretation of real structures. These features will be summarised and discussed below.

The doubly-plunging geometry of the fault-bend fold is responsible for the basic differences in kink-band width (in dip sections) and the linear decrease of structural height (in strike sections) observed in pre-tectonic sediments for both models (e.g. Figs. 4 and 7). Dip sections display classic pre-growth and growth strata geometries associated with fault-bend folds (cf. Suppe et al., 1991). In contrast, strike sections, depending on where they cut the structure, exhibit geometries very similar to those classically associated with symmetric detachment folds. The kink-band geometry and multiple panels observed in oblique sections reflect the

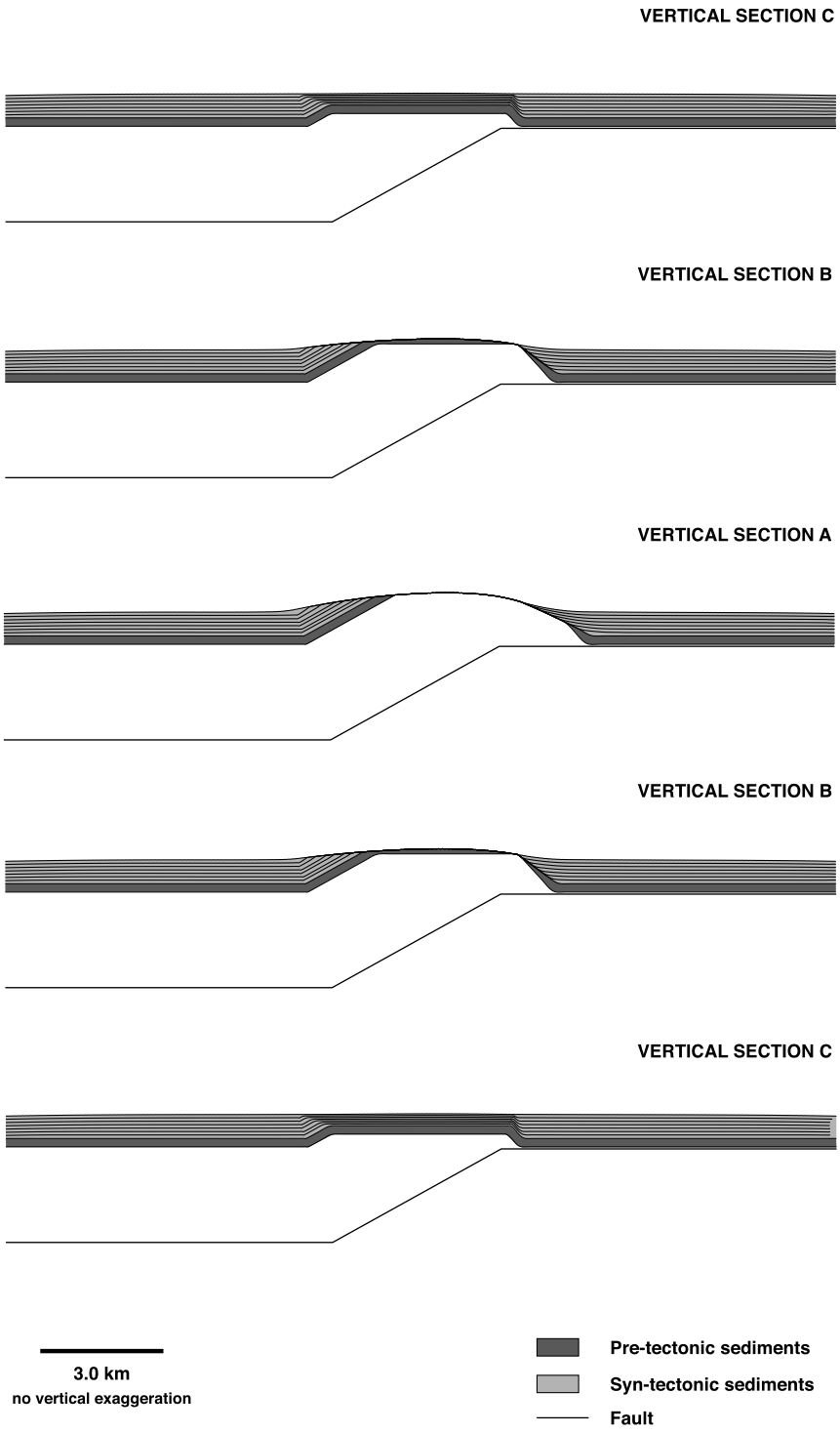

Fig. 9. Subaerial model with background sedimentation of 0.55 m/ka, maximum slip rate of 3.0 m/ka, and diffusion coefficient of 3000.0 m^2/ka. Growth strata are recorded at 150 ka intervals. (a) Vertical sections in the plane of the transport direction (dip sections). (b) Vertical sections in the plane perpendicular to the transport direction (strike sections). (c) Vertical sections at 45° to the transport direction (oblique sections).

doubly-plunging geometry of the fold as well as the orientation of the sections. The oblique sections display structural and stratigraphic geometries that contain both dip and strike components simultaneously.

For the 'fill-to-the-top' scenario, sections in the plane of the transport direction for both the *submarine* and *subaerial* models show the widest growth triangle in the central area and the narrowest at the boundaries, showing the doubly-plunging geometry of the anticline (Figs. 4a and 7a). A common feature is the change in attitude of growth axial

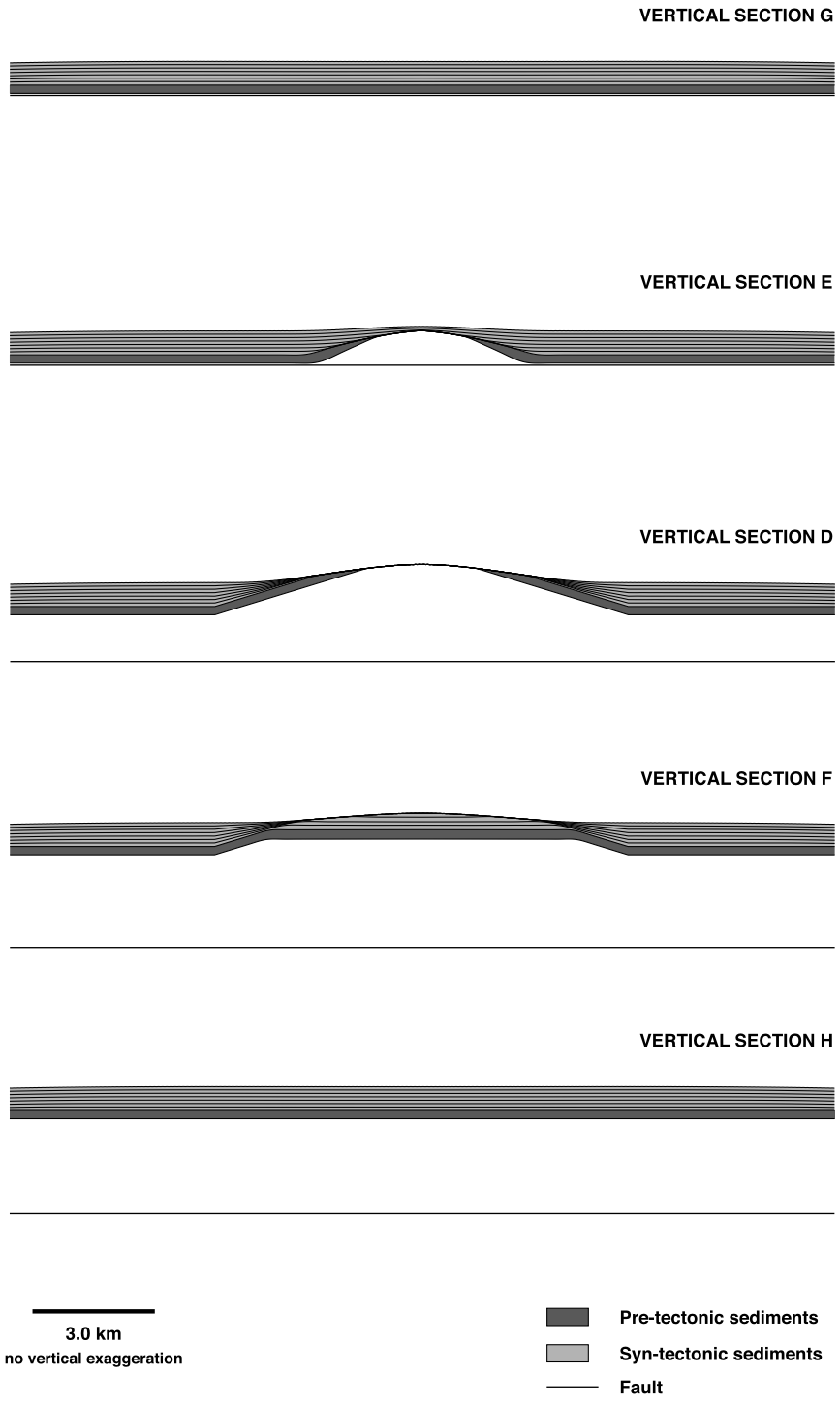

Fig. 9. (*continued*)

surfaces along the structure. In section A, the backlimb and forelimb growth axial surfaces rotate more toward the hinterland than those in vertical sections B and C. These geometries are associated with the accommodation space available in the system, which controls the change in sedimentation rate throughout the fault-bend fold. In the central area, the combination of tectonic uplift rate and base level change create an accommodation space value smaller than that at the margins. This situation creates an *effective sedimentation rate* that is relatively small in the central region, causing the rotation of growth axial surfaces toward the hinterland. Because of the accommodation space increases toward the boundaries of the fault-bend fold, the *effective*-sedimentation rate in this area is relatively high, and the growth axial surface shows less rotation towards the hinterland (see Figs. 4a and 7a). Thinning of syn-tectonic

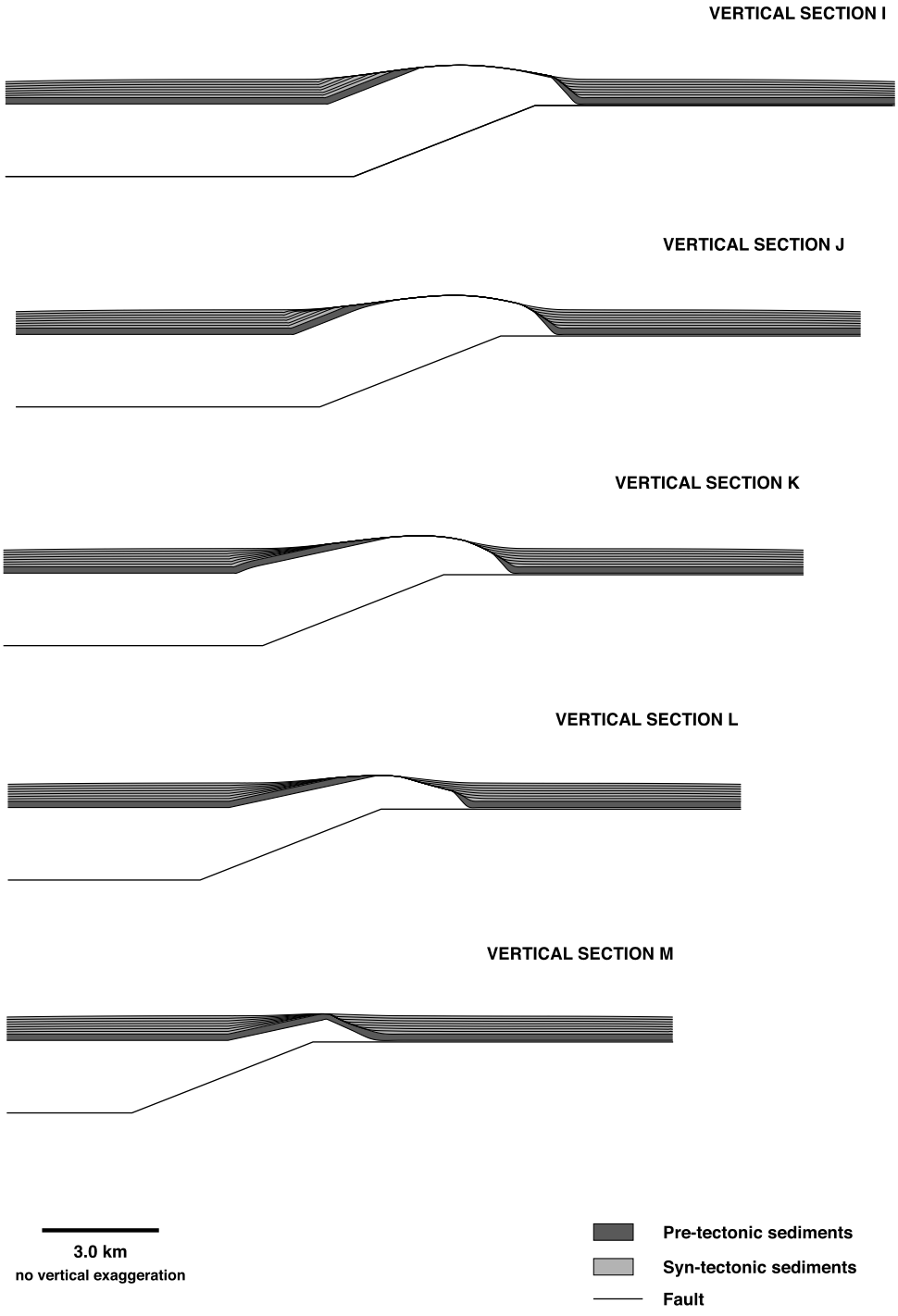

Fig. 9. (*continued*)

sediments along the structure and fanning are similar features shown by strike sections in both models (Figs. 4b and 7b). The thinning of growth strata reflects differences in accommodation space; low accommodation space in the central area and high accommodation space at the lateral margins of the fault-bend fold. This situation promotes a thick sedimentary sequence in the margin and a thin one in the centre. The fanning observed within syn-tectonic sediments is associated with tectonic activity. The older horizons have been involved in tectonic activity for a longer period of time and are folded more than the younger ones. The geometry of syn-tectonic sediments shown by oblique sections in both models (Figs. 4c and 7c) variably show growth triangles in the backlimb (sections I and J), forelimb (sections I–M) as well as thinning of growth strata over the crest of the anticline and fanning. In some oblique sections,

growth-strata geometries typically associated with kink-band migration and limb rotation are found together (e.g. Fig. 4c). The complex geometries observed within syn-tectonic sediments reflects the doubly-plunging geometry of the anticline and the orientation of sections.

Reducing the background sedimentation in the *submarine model* allows bathymetry to develop in the system (e.g. Figs. 5a and 6a). Similarly, a ridge develops in the *subaerial model* when aggradation rate is less than maximum uplift rate in the centre of the structure (e.g. Figs. 8a and 9a). The structural relief is accompanied by change in the geometry of syn-tectonic sediments; particularly, we observe evidence of unconformities where structural relief/bathymmetry are developed. Creation of bathymmetry or topographic relief is generally accompanied by erosion, transport and deposition, simulated here using the diffusion equation. Resultant geometries are smoother than 'fill-to-the-top' geometries, but nevertheless display many similar features.

The above discussion reinforces the idea of using 3D information in order to decipher the geometry of natural structures. Potential problems are minimised if we combine high quality 3D seismic data, outcrop and well information, but such data is not always available in every situation. A consistent feature of all the models is the rapid variation in growth-strata geometries between sections. This is particularly true where the sections are oblique or at right angles to the transport direction. These sections display complex structural/stratigraphic configurations that are not easily understood if the true 3D nature of the doubly-plunging fault bend fold is not taken into account.

6. Conclusions

A numerical scheme has been proposed to study the geometry of syn-tectonic sedimentation in a doubly-plunging, fault-bend fold anticline. The geometry of the syn-tectonic strata developed clearly reflects the interplay between stratigraphic and tectonic processes and base level change.

In both models studied, accommodation space and structural style (fault-bend folding) controls the basic geometry of growth structures. However, it has been shown that consideration of cross-section orientation is essential to prevent misinterpretation of growth strata geometries. In particular, we have shown that cross-sections oblique to the transport direction may contain complex and highly variable pre- and syn-tectonic geometries containing indications of both kink-band migration and limb rotation. The use of oblique 2D information to interpret 3D structures could cause misinterpretations if the complexities of stratigraphic configurations in three dimensions are not taken into account. This may not be of concern if there is a large amount of additional constraining information, but it is critical when 3D information is limited.

Acknowledgements

This study has benefited greatly from discussions with many colleagues; in particular Emma Finch, Enrique Novoa and Rob Gawthorpe. Critical comments by Josep Poblet and an anonymous reviewer helped greatly to improve this manuscript. Scott Wilkerson is especially thanked for his careful editorial comments and advice. Financial support for the study came from Norsk Hydro and PDVSA–INTEVEP, which is gratefully acknowledged.

References

Bezemer, T.-D., Kooi, H., Cloething, S., 1999. Numerical modelling of fault-related sedimentation. In: Harbaugh, J., Watney, W., Rankey, E., Slingerland, R., Goldstein, R., Franseen, E. (Eds.). Numerical Experiments in Stratigraphy: Recent Advances in Stratigraphic and Sedimentologic Computer Simulations. Special Publication 62, pp. 177–196 SEPM.

Chalaron, E., Mugnier, J.-L., Sassi, W., Mascle, G., 1996. Tectonics, erosion, and sedimentation in an overthrust system: a numerical approach. Computers and Geosciences 22, 117–138.

Colman, S.M., Watson, K., 1983. Ages estimated from a diffusion equation model for scarp degradation. Sciences 221, 263–265.

Flemings, P., Jordan, T., 1990. Stratigraphic modeling of foreland basins: Interpreting thrust deformation and lithosphere rheology. Geology 18, 430–434.

Ford, M., Williams, E., Artoni, A., Vergés, J., Hardy, S., 1997. Progressive evolution of a fault-related fold pair from growth strata geometries, Sant Llorenç de Morunys, SE Pyrenees. Journal of Structural Geology 19, 413–441.

Garcia-Castellano, D., Fernández, M., Torne, M., 1997. Numerical modeling of foreland basin formation: a program relating thrusting, flexure, sediment geometry and lithosphere rheology. Computers and Geosciences 23, 993–1003.

Gawthorpe, R.L., Sharp, I., Underhill, J.R., Gupta, S., 1997. Linked sequence stratigraphic and structural evolution of propagating normal faults. Geology 25, 795–798.

Gourlay, A., 1970. Hopscotch: a fast second-order partial differential equation solver. Journal of the Institute for Mathematic Applications 6, 375–390.

Hardy, S., 1994. Mathematical modelling of sedimentation in active tectonic settings. Ph.D. thesis, University of London.

Hardy, S., 1995. A method for quantifying the kinematics of fault-bend folding. Journal of Structural Geology 17, 1785–1788.

Hardy, S., Waltham, D., 1992. Computer modelling of tectonics, eustasy, and sedimentation using the Macintosh. Geobyte 7, 42–52.

Hardy, S., Poblet, J., 1995. The velocity description of deformation. Paper 2: sediment geometries associated with fault-bend and fault-propagation folds. Marine and Petroleum Geology 12, 165–176.

Jamison, J.W., 1987. Geometrical analysis of fold development in overthrust terranes. Journal of Structural Geology 27, 207–219.

Kenyon, P.M., Turcotte, D.L., 1985. Morphology of a delta prograding by bulk sediment transport. Geological Society of American Bulletin 96, 1457–1465.

Leeder, M., 1999. Sedimentology and Sedimentary Basins: from Turbulence to Tectonics. Blackwell Science Ltd, Oxford.

Poblet, J., Hardy, S., 1995. Reverse modelling of detachment folds; application to the Pico del Aguila anticline in the South Central Pyrenees (Spain). Journal of Structural Geology 17, 1707–1724.

Ramsay, J., 1991. Some geometric problems of ramp-flat thrust models. In: McClay, K.R. (Ed.). Thrust Tectonics. Chapman and Hall, London, pp. 191–200.

Shaw, J., Hook, S., Suppe, J., 1994. Structural trend analysis by axial

surface mapping. American Association of Petroleum Geologists Bulletin 78, 700–721.

Suppe, J., 1983. Geometry and kinematics of fault-bend folding. American Journal of Science 283, 684–721.

Suppe, J., Chou, G., Hook, S., 1991. Rates of folding and faulting determined from growth strata. In: McClay, K.R. (Ed.). Thrust Tectonics. Chapman and Hall, London, pp. 105–121.

Waltham, D., 1992. Mathematical modelling of sedimentary basin processes. Marine and Petroleum Geology 9, 265–273.

Waltham, D., Hardy, S., 1995. The velocity description of deformation. Paper 1: theory. Marine and Petroleum Geology 12, 153–163.

Wilkerson, S., 1992. Differential transport and continuity of thrust sheets. Journal of Structural Geology 14, 749–751.

Wilkerson, S., Medwedeff, D., Marshak, S., 1991. Geometrical modeling of fault-related folds: a pseudo-three-dimensional approach. Journal of Structural Geology 13, 801–812.

Zoetemeijer, R., Sassi, W., Roure, F., Cloeting, S., 1992. Stratigraphic and kinematic modeling of thrust evolution, northern Apennines, Italy. Geology 20, 1035–1038.

Zoetemeijer, R., Cloeting, S., Sassi, W., Roure, F., 1993. Modelling of piggyback-basin stratigraphy: record of tectonic evolution. Tectonophysics 226, 253–269.